

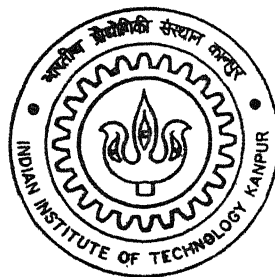
4110511

FINITE ELEMENT ANALYSIS OF DYNAMIC ELASTO-PLASTIC CONTACT PROBLEM WITH FRICTION

By

Jayadeep U. B.

TH
ME/2003/M
J 335 f



DEPARTMENT OF MECHANICAL ENGINEERING
Indian Institute of Technology Kanpur
FEBRUARY, 2003

FINITE ELEMENT ANALYSIS OF DYNAMIC ELASTO-PLASTIC CONTACT PROBLEM WITH FRICTION

A Thesis Submitted
in Partial Fulfillment of the Requirements
for the Degree of
Master of Technology

by
JAYADEEP U. B.



to the
DEPARTMENT OF MECHANICAL ENGINEERING
INDIAN INSTITUTE OF TECHNOLOGY KANPUR
FEBRUARY, 2003

30 MAY 2003

पुरुषोत्तम कर्मानाथ कोल्हकर पुस्तकालय

भारतीय प्रौद्योगिकी संस्थान कानपुर

अवधि क्र० A 143+11



CERTIFICATE

29/02/03
I.I.T. KANPUR/6870

It is certified that the work contained in the thesis entitled “*Finite Element Analysis of Dynamic Elasto-plastic Contact Problem with Friction*”, by Jayadeep U. B., has been carried out under my supervision and that this work has not been submitted elsewhere for a degree.



Dr. P. M. Dixit

February, 2003.

Department of Mechanical Engineering,

I.I.T. Kanpur.

Abstract

A finite element code is developed for solving 3-D, dynamic, elasto-plastic, contact problem, including the effects of friction at the contact interface. Elasto-plastic behaviour is modelled by an associated flow rule based on the von Mises yield criterion and power law type isotropic hardening. Jaumann stress rate tensor and incremental Green-Lagrange strain tensor are used as the objective stress and non-linear strain measures respectively. The material and geometric non-linearities are handled by using the updated Lagrangian method. A node-to-segment interface model is used for developing the contact stiffness matrix. Contact constraints are imposed using Lagrange multiplier method. Coulomb's friction law is used for calculating the friction forces. A finite element – finite difference scheme is used for spatial and temporal discretization respectively and Modified Newton-Raphson iteration method is used for solving the non-linear governing equation. To improve the convergence characteristics of Newton-Raphson iterations, under-relaxation technique and line search method are used. The finite difference scheme used for time integration is Newmark's algorithm. Unloading is incorporated to include the effects of global or local unloading during the analysis. Skyline scheme of assembly and static condensation scheme are used to reduce the computational resources required for the analysis. The finite element code is validated using three standard problems from the published literature. Finally, a 3-D, dynamic, elasto-plastic contact problem with friction is solved to demonstrate the applicability of the code.

Acknowledgements

First and foremost, I express my deep sense of gratitude to my thesis supervisor **Dr. P. M. Dixit**. Without his able guidance and ample support, this work would not have been materialized. His systematic approach to all matters has been a significant influence on my way of working. The lessons learned during the close interaction, which I had with him for the past one year, will guide me in all my future endeavours.

I express my gratitude to all my teachers, who helped me to accomplish this cherished dream of doing post-graduation and to my family members, who always encouraged me to pursue my interests.

The fantastic atmosphere and cooperation extended by my labmates, Sachin, Santosh and Rajiv, at **FEAL** (Finite Element Analysis Lab), helped to make this thesis work a pleasant experience.

I would like to thank my seniors, Pathari, Pradeep, Tony, Rajesh and David sir, for their guidance during the initial days of my life at IITK. The life here would not have been so memorable without my great friends, particularly, Manoj, Kartha, Thottan, Visakh, Sreejit and Holla.

Last, but by no means the least, the financial support provided by **ADA** (Aeronautical Development Agency) for this work is gratefully acknowledged.

Jayadeep U. B.,
I.I.T. Kanpur,
February, 2003.

Contents

Certificate	i
Abstract	ii
Acknowledgements	iii
List of Figures	vii
List of Symbols	ix
1 Introduction	1
1.1 Review of Literature	1
1.1.1 Elasto-plastic Finite Element Analysis	3
1.1.2 Dynamic Finite Element Analysis	4
1.1.3 Contact Analysis	5
1.2 Objective of the Present Work	8
1.3 Structure of the Thesis	9
2 Mathematical Modeling of Dynamic Elasto-Plastic Problem	10
2.1 Introduction	10
2.2 Stress Measures	11
2.3 Strain Measures	12
2.4 Elastic Constitutive Equation	12
2.5 Elasto-plastic Constitutive Equation	13
2.6 Incremental Updated Lagrangian Formulation	15
3 Finite Element-Finite Difference Formulation	18
3.1 Matrix Notation	18

3.2	Finite Element Formulation	20
3.3	Finite Difference Scheme	22
3.4	Determination of Stress	24
3.4.1	Integration of the Constitutive Equation	25
3.4.2	Unloading Scheme	26
3.5	Skyline Scheme of Global Assembly	26
3.6	Static Condensation Scheme	27
3.7	Modified Newton-Raphson Scheme	29
3.8	Divergence Handling Procedures	29
3.9	Numerical Aspects	31
3.9.1	Choice of Time-step	31
3.9.2	Deformation Dependent Loading	32
3.9.3	Stress Updation	33
4	Contact Formulation	34
4.1	Contact Constraints	34
4.2	Contact Force Expressions	37
4.2.1	Sticking Friction Condition	38
4.2.2	Slipping Condition	39
4.3	Kinematic Constraints in Nodal Form	40
4.3.1	Sticking Friction Condition	40
4.3.2	Slipping Condition	42
4.4	Lagrange Multiplier Method	42
4.5	Algorithm used for Dynamic Large Deformation Elasto-plastic Contact Problem	43
5	Results and Discussion	46
5.1	Validation	46
5.1.1	Elasto-plastic Dynamic Response of a Simply Supported Square Plate	47
5.1.2	Oblique Impact of Two Infinite Blocks	50
5.1.3	Impact of two Cantilever Beams	54
5.1.4	Elasto-plastic Impact of a Sphere on a Plate with Friction	58

6	Conclusions and Scope for Future Work	69
6.1	Conclusions	69
6.2	Scope for Future Work	70
		71
	References	

List of Figures

4.1	Two body contact system	35
4.2	Points in contact and associated normal and tangent vectors	36
5.1	Displacement at the center of the plate (Ref. [49])	48
5.2	Displacement at the center of the plate (Present work)	48
5.3	Maximum equivalent stress in the plate (Present work)	49
5.4	Maximum equivalent plastic strain in the plate (Present work)	49
5.5	Oblique impact of two elastic blocks	50
5.6	X-displacement of point P (Ref. [43])	52
5.7	X-displacement of point P (present work)	52
5.8	Y-displacement of point P (Ref. [43])	53
5.9	Z-displacement of point P (Present work)	53
5.10	Impact of two cantilever beams	54
5.11	Horizontal displacement at the end tip of upper cantilever (Ref. [35]) . . .	56
5.12	Horizontal displacement at the end tip of upper cantilever (Present work) .	56
5.13	Vertical displacement at the end tip of upper cantilever (Ref. [35])	57
5.14	Vertical displacement at the end tip of upper cantilever (Present work) . .	57
5.15	Impact of a sphere on plate	58
5.16	Finite element plot of sphere (Full view)	59
5.17	Finite element plot of sphere (Sectional view in X-Z plane)	60
5.18	Impact of sphere on plate (Frictionless): Configuration at $t = 0.0$	61
5.19	Impact of sphere on plate (Frictionless): Configuration at $t = 0.02$	62
5.20	Impact of sphere on plate (Frictionless): Configuration at $t = 0.04$	62
5.21	Impact of sphere on plate (Frictionless): Configuration at $t = 0.06$	63
5.22	Impact of sphere on plate (Frictional): Configuration at $t = 0.0$	63
5.23	Impact of sphere on plate (Frictional): Configuration at $t = 0.02$	64

5.24	Impact of sphere on plate (Frictional): Configuration at $t = 0.04$	64
5.25	Impact of sphere on plate (Frictional): Configuration at $t = 0.06$	65
5.26	Displacement of the sphere along X -direction	65
5.27	Displacement of the sphere along Z -direction	66
5.28	Maximum equivalent stress in sphere and plate	66
5.29	Displacement of the sphere along X -direction (polycarbonate material) . .	67
5.30	Displacement of the sphere along Z -direction (polycarbonate material) . .	67
5.31	Maximum equivalent stress in sphere and plate (polycarbonate material) .	68

$[K_N]$	Non-linear part of stiffness matrix
$[K_d]$	Effective stiffness matrix
$[\widehat{K}]$	Condensed form of stiffness matrix
L_e	Effective length
$[M]$	Mass matrix
n	Hardening exponent
N_i	Shape function
$\underline{N_1}$	Outward normal vector
$\underline{N_2}, \underline{N_3}$	Tangential vectors
$\{N_1\}, \dots$	Array forms of direction vectors
P	Penetration
$[Q]$	Matrix containing the shape functions of the element
$\{R\}$	Unbalance force vector
$\{R_c\}$	Contact force vector
S_{ij}	Second Piola-Kirchoff stress tensor
$[S]$	Matrix representation of Second Piola-Kirchoff stress tensor
S_F	Surface where tractions are specified
S_D	Surface where displacements are specified
S_C	Surface where contact occurs
t	Time
t_i	Traction
tol_c	Tolerance for convergence of the numerical method
u^i	Displacement of node i specified in the X-direction
$\{U_1\}$	Displacement vector corresponding to nodes of type 1
$\{U_2\}$	Displacement vector corresponding to nodes of type 2
$\{U\}$	Global displacement vector
$\{\widehat{U}\}$	Condensed form of displacement vector
$\{\dot{U}\}$	Global velocity vector
$\{\ddot{U}\}$	Global acceleration vector
v^i	Displacement of node i specified in Y-direction
V	Volume
w^i	Displacement of node i specified in Z-direction

Ω_{ij}	Spin tensor
x_i	Co-ordinate of generic particle
α, δ	Newmark parameters
δ	Variation symbol
δ_{ij}	Kronecker delta
${}_t\Delta$	Increment in quantity from t to $t + \Delta t$
ε_{ij}	Small strain tensor
$[\varepsilon]$	Matrix representation of small strain tensor
ε_{eq}^p	Equivalent plastic strain
η_{ij}	Non-linear part of the Green-Lagrange strain tensor
λ, μ	Lame's constants
μ	Coefficient of friction
ν	Poisson's ratio
ρ	Density
σ_{ij}	Cauchy stress tensor
$[\sigma]$	Matrix representation of Cauchy stress tensor
$\dot{\sigma}_{ij}$	Cauchy stress rate tensor
$\overset{\circ}{\sigma}_{ij}$	Jaumann stress rate tensor
σ_y	Yield stress
σ'_{ij}	Deviatoric part of the Cauchy stress tensor
$\{\Phi_i\}$	Array of shape functions
θ	Angle between resultant tangential force $\{f_t\}$ and $\{N_2\}$

Superscripts and Subscripts

tX	Quantity X evaluated at time t
${}^{t+\Delta t}X$	Quantity X evaluated at time $t + \Delta t$
${}^{t+\Delta t}_tX$	Quantity X evaluated at time $t + \Delta t$ based on coordinates at t
X_{ij}	Row i and column j element of Matrix/Tensor X

Chapter 1

Introduction

Contact interactions occur in virtually all structural and mechanical systems. They can be intentional as in the case of transfer of loads between two components or unintentional as in a vehicle crash. If the contacting bodies are not in static equilibrium during the contact, then it is called a dynamic contact or impact. The basic characteristics of a dynamic contact phenomenon are very brief duration, high force levels reached, rapid dissipation of energy and large accelerations and decelerations present. By nature, the contact phenomenon always involve friction. In many cases, the bodies undergo plastic deformations during contact. A rigorous analysis of the contact problem requires the consideration of all these complex aspects. The analysis of the problems like the automobile crashes involves the use of dynamics, elasto-plasticity and large deformation in a contact analysis scenario.

Closed form mathematical solutions are extremely difficult to develop even for simple contact problems. As the contact scenario becomes more complex, as in the case of elasto-plastic materials, arriving at a closed form solution is nearly impossible. This necessitates the use of approximate numerical tools for the analysis, of which finite element analysis is arguably the most versatile option. .

1.1 Review of Literature

The classical incremental theory of elasto-plasticity [1] is generally taken to be the basis for predicting elasto-plastic response. The constitutive equation for these materials are derived by combining the stress-strain relations for elastic and plastic response. The constitutive relation for a plastic response requires three fundamental characteristics of

the material: a *yield criterion*, a *flow rule* and a *strain hardening relationship*. The yield criterion demarcates the elastic behaviour from the plastic behaviour. It specifies the state of multi-axial stress corresponding to the start of the plastic flow. Various yield criteria have been proposed by Tresca, von Mises etc. [2], where von Mises criterion is found to be the simplest and the most accurate in terms of the predicted values. The flow rule relates the plastic strain rate to the current stress. It is represented in terms of a plastic potential, analogous to the elastic potential, and is termed as the *associated flow rule* if the potential is taken as the yield function. The hardening rule specifies how the yield condition is modified during the plastic flow. For the purpose of analysis, the non-linear hardening relationship is usually modelled in terms of a *power law*.

Unlike the case of small deformation of elastic materials, the governing equations of elasto-plastic materials, which undergo large deformation, contain two types of non-linearities: (i) *geometric non-linearity* associated with non-linear strain displacement relations and (ii) *material non-linearity* in the form of non-linear stress-strain relations. An incremental formulation like the *Updated Lagrangian Formulation* is the most convenient way to handle such non-linearities unlike the total Lagrangian formulation. The advantage of the former is that, if the increment size is sufficiently small, linearized incremental equations can be used. However, when the overall deformation is large, the number of increments is to be prohibitively large. In such a situation, we have to resort to some iterative scheme for solving the non-linear incremental equations. The prominent among such schemes is the *Newton-Raphson method*. In this method, the stiffness matrix is updated in each iteration of the increment. Thus, we work with the tangent modulus at that instant for each iteration. This method has two shortcomings. The first being that there is chance of divergence if the slope of force-displacement curve increases with the increment. Secondly, it takes more computational time as the stiffness matrix has to be computed afresh in each iteration [3]. Thus, the *Modified Newton-Raphson method* in which, the stiffness matrix is kept constant during the increment, is adopted.

The dynamic analysis is very basic to studying impact problems. There are various ways of performing the time discretization in this category of problems of which, the direct integration methods are prominent. These methods include the central difference method, Houbolt method, Wilson- θ method and Newmark method [4]. The first method is conditionally stable one, while the rest of them are unconditionally stable. Analysis of accuracy and speed of different algorithms is presented by Bathe [4]. It has been

concluded that although central difference method is beneficial in terms of speed and cost, the trapezoidal method of Newmark's algorithm is best in terms of stability and accuracy.

1.1.1 Elasto-plastic Finite Element Analysis

As stated earlier, the classical theory of elasto-plasticity [1] is generally taken to be the basis for predicting the elasto-plastic response. Argyris [5] presented one of the earliest formulations and solution techniques for elasto-plastic problems. The effect of plasticity was simulated by "initial loads" and the matrix method was used to discretize the linearized governing equations. Two approaches, the direct incremental method and the iterative incremental method, were discussed for obtaining the solution. The early applications of the iterative incremental method [3] used the initial stiffness method. However, this approach is not suited when the overall deformation is very large as it results in very slow convergence, or in many cases, even divergence.

Nagtegaal and Jong [6] dealt with the computational aspects of elastic-plastic large deformation analysis. A modified set of governing equations were formulated, which were applicable for small strain and large rotational increments. Special attention was paid to the integration of these equations in the deformation history. It is predicted that explicit methods, like the tangent modulus procedure, are conditionally stable whereas the implicit schemes, such as the mean normal method, are preferable. The main difficulty with the three dimensional analysis is the vast computational memory that it requires. But, with the advent of better machines and evolution of more efficient algorithms this problem has been solved and more and more such analyses are being carried out.

Since the elasto-plastic constitutive relation is generally given in the differential form, the constitutive function must be integrated to obtain the incremental stress. The procedures commonly used are the simple and robust Euler forward integration technique, the implicit Euler backward integration technique and the radial return method. The trend has lately been shifting towards the use of consistent schemes which improve the convergence characteristics of the equilibrium iterations [7].

Bathe [4] has briefly reviewed the different approaches used for obtaining the solution of general non-linear problems. Total and updated Lagrangian descriptions of motion have been used to formulate the incremental equations of motion. It has been noticed, for

the problems solved, that the two formulations give identical results, provided appropriate constitutive relations are used. One of the areas of controversy in analyzing large deformation is the choice of appropriate objective stress measures. Various objective stress measures have been discussed by Bathe [4] and Chakrabarty [8]. The classical theory of elasto-plasticity assumes that the incremental strain tensor can be additively decomposed into the elastic and plastic parts. While this may be true for small incremental deformation, this assumption is no longer valid for large incremental strains and rotations, unless appropriate strain measures are used [9, 10] .

1.1.2 Dynamic Finite Element Analysis

Bathe *et al* [11] were probably the first to propose a large deformation dynamic finite element formulation. Total and updated Lagrangian descriptions of motion were used to formulate the incremental equations of motion. A detailed finite element analysis of non-linear static and dynamic response was also carried out by Mondkar and Powell [12]. The purpose of this paper was to review the theoretical and computational techniques for non-linear structural analysis, and their applications in a general computer program. A Lagrangian frame of reference was used and a variational form of the incremental equations of motion for large displacement, finite strain deformation was incorporated in the finite element program. It was found that no specific time integration scheme was optimal for all types of non-linear behaviour. It was inferred that for large load steps it was essential to use iterations to obtain accurate results.

Direct integration methods are the most commonly used methods for solving the discretized and linearized governing equations of motion. Dynamic equilibrium including the effect of damping forces is sought at discrete time instants instead of at all times. The advantage is obvious: all solution techniques employed in static analysis can probably be used most effectively in direct integration. The selection of any one direct integration methods depends upon considerations of accuracy, stability and cost. The importance of using equilibrium iterations in dynamic non-linear analysis was first realized by Bathe [4]. An extensive discussion of these and other methods can be found in Bathe [4].

More recently, Gendy and Saleeb [13] found that, for a more comprehensive perspective, work on the non-linear dynamic responses of plates and shells calls for detailed studies of several important factors. These include the effect of large spatial rotations on

the geometric stiffness and inertia operators, accurate updating procedures for nodal rotations and associated angular velocities and accelerations, as well as material inelasticities (especially for finite strains). Several of these issues were examined in conjunction with a newly developed mixed finite element formulation for plates and shells. To this end, and restricting the scope to the case of large overall motions but small strains, low-order displacement/strain interpolations are utilized, together with a radial return algorithm (backward Euler-integration scheme) for plasticity effects. The Newmark implicit scheme has been employed to integrate the semi-discrete equations of motion.

1.1.3 Contact Analysis

The analysis of contact has been a fascinating area since the initial days of the study of mechanics itself. Many investigators tried to determine the stresses and displacements in two elastic bodies coming in contact. In three dimensions, the problem of two contacting elastic bodies was first formulated and solved by Hertz [14] under several restrictive assumptions. Hertz assumed that the geometry of general curved surface in the vicinity of contact can be described by quadratic terms only. Neglecting friction and assuming that the bodies in contact deform as though they were elastic half-spaces, Hertz used the Boussinesq solution to deduce that the contact pressure distribution has to be elliptical to produce an elliptical area. For the contact between two spheres, the contact area is circular. Research work based on Hertz's theory up to 1982 has been reviewed by Johnson [15]. Although Hertz evaluated the dimensions of contact area and stresses at the contact surface, he presented only a speculative sketch of the subsurface stresses. The stresses beneath the contact surface were analyzed later. For circular contact area of radius a , it was observed that the maximum shear stress occurs at a depth of $0.57a$ [15]. Later on Muskhelishvili [16] and Gladwell [17] solved some small deformation elastic contact problems using the analytical techniques.

With the development of computers, people resorted to numerical methods. Finite element method has been the most widely used. In earlier studies, contacting bodies were assumed to consist of linearly elastic materials and hence were assumed to undergo only small deformation. The loading was assumed to be proportional. The node-to-node contact interface model was used for discretizing the contacting bodies and the contact conditions (constraints) involving nodal displacements and forces were applied

by modifying the combined stiffness matrix or the flexibility matrix of the contacting bodies. The investigators who used this model are Ohte [18], Gaertner [19], Francavilla and Zienkiewicz [20], Sachdeva and Ramakrishnan [21] etc.

Kalker and Randen [22], Hung and de Saxce [23] and Mahmoud *et al.* [24] used the technique of mathematical programming for solving the frictionless small deformation elastic contact problem. They minimised the total strain energy to find the contact area and the contact pressure distributions.

When the deformation is large, there is possibility that a pair of nodes presently in contact, may undergo a large relative displacement. If a node-to-node interface model is used, re-meshing of the bodies becomes necessary for carrying out the subsequent analysis. To avoid frequent re-meshing, one must use the node-to-segment interface model, in which one node of a contacting body comes in contact with a segment of the other. When a node-to-segment interface model is used, the contact conditions acquire a complex form, when expressed in terms of nodal variables. To impose these conditions, an additional set of finite element equations, involving the *contact stiffness matrix*, needs to be developed using the principle of virtual work of the contact forces. The methods, which are normally used for implementing the contact constraints are *Lagrange multiplier method*, *penalty function method* and *transformation matrix method*. Bohm [25] presented a comparison of different contact algorithms with applications. A survey of contact algorithms is given by Bourago [26].

Kikuchi and Oden [27] have provided the mathematical foundation for the Lagrange multiplier method. The work of Bathe and Chaudhary [28] seems to be the first attempt to develop an expression for contact stiffness matrix using this method. This was done for planar and axisymmetric problems assuming the contact segment to be straight. Lagrange multiplier was used to impose the contact constraints including friction forces based on *Coulomb's friction law*. Non-linear contact kinematics was used for developing a consistent contact matrix for two dimensional problems by Wriggers and Simo [29] and by Parisch [30]. They used both the Lagrange multiplier method and penalty function method. The transformation matrix method for two dimensional problems was proposed by Chen and Yeh [31]. A formulation for non-linear frictional model was proposed by Gallego and Anza [32] using perturbed Lagrangian functional. All the above formulations were used for static large deformation elastic contact problems. Some of these formulations were extended to elasto-dynamic contact problems [4, 29] and dynamic elasto-plastic

problems [33]. A literature survey of contact dynamics modelling is presented by Gilardi and Sharf [34]. Sung and Kwak [35] and Bittencourt and Creus [36] present the analysis of dynamic, large deformation contact including the effects of friction. Master's thesis by Werner [37] is an attempt to compare the experimental results and the results predicted by a commercial finite element software for an elasto-plastic impact problem.

Contact-impact algorithms, which are sometimes called as *slideline algorithms*, are the computationally time-consuming parts of many explicit simulations of non-linear problems, because they involve so many branches, and so are not amenable to vectorization, which is essential for speed on supercomputers. Belytschko and Neal [38] introduced the pinball algorithm, which is a simplified slideline algorithm and is readily vectorized. Its major idea is to embed pinballs in surface elements and to enforce the impenetrability condition only to these pinballs. It can be implemented either by a Lagrange multiplier or penalty method. Malone and Johnson [39] developed a parallel contact algorithm and implemented it in a non-linear dynamic explicit finite element program to analyze the three-dimensional shell structures. The contact algorithm accounted for initial contact, sliding and release through the use of parametric representation of motion of points located on the surface of structure combined with a contact surface representation, which approximates the actual surface by means of triangular search planes. Brown *et al.* [40] described a general strategy for parallelizing solid mechanics simulations. Such simulations often have several computationally intensive parts, including finite element integration, detection of material contacts and particle interactions if smoothed particle hydrodynamics is used to model highly deforming materials. Their strategy is to load-balance each of the significant computations independently with whatever balancing technique is most appropriate. The main advantage is that each computation can be scalably parallelized. The drawback is the data exchange between the processors and the extra coding that must be written to maintain multiple decompositions in a code.

The problems of undesirable oscillatory solutions and stability of time-integration schemes have been tackled by quite a few people. Taylor and Papadopoulos [41] address the problem of oscillatory solution along the contact interface. The standard second order implicit integrators of the Newmark family, used in earlier works, were examined by them. In their work, control of these oscillations is attempted by introducing an artificial bulk viscosity for the compressive waves in each body. Laursen and Chawla [42] proposed an energy conserving algorithm to control the oscillations for the frictionless dynamic contact

problems. It is shown that a Lagrange multiplier enforcement of an appropriate *contact rate constraint* produces these conservation properties. In particular, the ability of the formulation to produce accurate results, where more conventional integration schemes fail, is emphasized by numerical simulations. Armero and Petocz [43] presented a new dissipative time-stepping algorithm to improve the stability of time integration scheme. They showed that although the traditional time-integration schemes were stable for most of the linear problems, instability would creep in as soon as we try to use them in non-linear cases. Given these considerations, they developed implicit time-stepping algorithms for contact problems that possess unconditional (energy) stability in time and lead to stable enforcement of contact constraints.

Quite a few researchers have proposed new techniques. Ayari and Saouma [44] developed a new formulation for contact problems using the concept of fictitious forces. Contrary to the most existing models, this one involves very few matrix decompositions and thus is computationally inexpensive. The model was applied to fracture mechanics based analysis of a cracked dam under seismic excitation. They also showed that their model could be applied to a vast majority of contact problems and was not only restricted to fracture phenomenon. Simo and Laursen [45] extended the augmented Lagrangian formulation, which has certain advantages over traditional Lagrangian formulation, to problems involving frictional contact. Kane *et al* [46] proposed a nonsmooth contact algorithm, which is capable of dealing with multibody nonsmooth contact geometries for which neither the normals nor the gap functions can be defined. Farahani *et al* [47] presented a solution method for contact/impact problems, which is different from Lagrange multiplier and penalty methods. This method is based on the stiffness matrix transformation and eliminating the normal degree of freedom of contactor node. The method is absolutely general and can be used in static as well as dynamic non-linear problems. In this case, the number of unknowns does not increase and the solution scheme needs no modification as is the case with prior methods. Besides, the boundary conditions are satisfied exactly.

1.2 Objective of the Present Work

The objective of the present work is to develop an efficient finite element software for large deformation, dynamic, elasto-plastic contact problem including the effects of friction at the contact interface. Since we have large deformations, including slipping

at the contact interface, a node-to-segment contact model is used in contact analysis. A method outlined by Zhong [33] is used for calculating the contact stiffness matrix. Lagrange multiplier method is used for applying the contact constraints as penalty method is found to be dependent on the penalty number, which is a *free* (user defined) parameter. Coulomb's friction law is used for modelling the frictional effects at the contact interface.

Elastic behaviour is modelled using generalised Hooke's law and the plastic behaviour is modelled by an associated flow rule based on von Mises yield criterion and power-law type isotropic hardening. The total strain is obtained by adding the elastic and plastic components. Jaumann stress rate tensor and incremental Green-Lagrange strain tensor are used as objective stress and non-linear strain measures in the formulation of constitutive equations. Incremental analysis is carried out using the updated Lagrangian method [4]. Modified Newton-Raphson iterative method is used for solving the resulting finite element equation. In each Newton-Raphson iteration, contact iterations are carried out to find the contact reactions. A finite difference scheme is used for carrying out the discretization in time. Newmark's algorithm, which is found to be the best in terms of stability and accuracy among the various finite difference schemes, is used for this purpose. Unloading scheme is incorporated to take care of the local unloading during the analysis. To reduce the computational resources required for performing the analysis, static condensation of stiffness matrix for contact and non-contact nodes and skyline scheme of assembly are used. Divergence handling techniques, viz., under relaxation and line search, are used for improving the convergence characteristics of Newton-Raphson iterations.

1.3 Structure of the Thesis

Chapter 2 deals with the mathematical formulation of the governing equations for dynamic, large deformation, elasto-plastic problems. The development of the finite element-finite difference scheme based on these governing equations and the numerical scheme used are discussed in chapter 3. Chapter 4 presents the contact formulation, wherein the formulation of the contact stiffness matrix and the calculation of contact reactions are discussed. Chapter 5 is devoted for the results of the validation problems used for validating the code and an additional problem to show the capabilities of the finite element code. The last chapter summarises the work carried out and the scope for future developments.

Chapter 2

Mathematical Modeling of Dynamic Elasto-Plastic Problem

In a dynamic elasto-plastic problem, the deformations and strains in the body no longer remain small and hence the response of the body is not proportional to the load. The response of the body becomes non-linear. The non-linearities can be broadly classified into two: *Geometric non-linearity* and *material non-linearity*. Both these non-linearities occur in the analysis of large deformation of elasto-plastic materials. The most convenient formulation for such analysis is the *Updated Lagrangian Formulation* with the constitutive relations represented in an incremental manner.

2.1 Introduction

In the study of the deformation of a body subjected to external loading, often the original, undeformed and unstressed state of the body is used for the formulation of its governing equation. This method is known as the Lagrangian formulation. This formulation is convenient for small deformation problems, where the deformed configuration does not deviate from the original configuration significantly. Hence, the deformations are proportional to the loading and can be described by an infinitesimal or linear strain tensor, for which the strain – displacement relations are linear. On the other hand, for large deformation problems, one has to use a finite strain measure, which is expressed by a non-linear strain displacement relation. Furthermore, the equations of motion, expressed in the original configuration, depend on the deformation. This makes the governing equations highly complex and too difficult to solve. In such cases, it is convenient to solve

the problem in an incremental manner known as the *Updated Lagrangian Formulation*. In this formulation, the state of the body is updated in increments using the calculated incremental deformations and stresses. The response during Δt is calculated based on the configuration at time t , where Δt represents the increment in time, called *time step*. Hence, all the relations are to be in an incremental form rather than the total form. This methodology is particularly useful for elasto-plastic materials, since the constitutive relations for these materials depend on the state of the body and therefore they are expressed in an incremental form.

2.2 Stress Measures

The large deformation problems are normally associated with rigid body rotations. Hence the stress measures used in these problems should be *objective*, which means that they should vanish if the increment is a pure rigid body rotation. The most commonly used stress measure known as *Cauchy stress tensor* is not objective and hence it can not be used in a constitutive equation. There are numerous objective stress measures, of which two are discussed below.

One of the commonly used objective stress measures is the *second Piola-Kirchoff stress tensor* ${}^{t+\Delta t}_t S_{ij}$ which is related to Cauchy stress tensor ${}^{t+\Delta t}_t \sigma_{mn}$ using the concept of equivalent work between the two configurations [4]:

$${}^{t+\Delta t}_t S_{ij} = \frac{{}^t \rho}{{}^{t+\Delta t}_t \rho} \cdot {}^{t+\Delta t}_t x_{i,m} \cdot {}^{t+\Delta t}_t \sigma_{mn} \cdot {}^{t+\Delta t}_t x_{j,n} \quad (2.1)$$

Here ${}^t \rho$ and ${}^{t+\Delta t}_t \rho$ represent the densities at time t and time $t + \Delta t$ respectively, ${}^{t+\Delta t}_t x_{i,m}$ is the derivative of the position vector at time t , viz., ${}^t x_i$ with respect to ${}^{t+\Delta t}_t x_m$. Another frequently used objective stress measure is *Jaumann's stress rate tensor* ${}^t \overset{\circ}{\sigma}_{ij}$. It is related to the Cauchy rate $\dot{\sigma}_{ij}$ by the relation [4]:

$${}^t \overset{\circ}{\sigma}_{ij} \Delta t = \dot{\sigma}_{ij} \Delta t - {}^t \sigma_{ik} ({}^t \Omega_{jk} \Delta t) - {}^t \sigma_{jk} ({}^t \Omega_{ik} \Delta t) \quad (2.2)$$

$${}^t \Omega_{jk} \Delta t = \frac{1}{2} ({}_t \Delta u_{i,j} - {}_t \Delta u_{j,i}) \quad (2.3)$$

Here, ${}^t \Omega_{jk} \Delta t$ represents the incremental spin tensor and ${}_t \Delta u_{i,j}$ denotes the derivative of the incremental displacement vector ${}_t \Delta u_i$ with respect to ${}^t x_j$.

The second Piola-Kirchoff stress tensor is energy conjugate to the Green-Lagrange strain tensor. Therefore, it is used in this work to develop the virtual work expressions in Updated Lagrangian formulation, whereas for developing the elasto-plastic constitutive equations, the Jaumann stress rate tensor, which is closely related to Cauchy stress rate, is used.

2.3 Strain Measures

The linear or infinitesimal strain tensor, normally used in the small deformation problems, is not a valid choice for the large deformation, elasto-plastic analysis. *Green-Lagrange strain tensor* is one of the most commonly used strain measure for large deformation analysis.

The incremental Green-Lagrange strain tensor is a non-linear function of the displacement [4]:

$${}_t\Delta e_{ij} = \frac{1}{2}({}_t\Delta u_{i,j} + {}_t\Delta u_{j,i} + {}_t\Delta u_{k,i} {}_t\Delta u_{k,j}) \quad (2.4)$$

When the incremental deformation is small, the incremental linear strain tensor

$${}_t\Delta \epsilon_{ij} = \frac{1}{2}({}_t\Delta u_{i,j} + {}_t\Delta u_{j,i}) \quad (2.5)$$

can be used as the measure of deformation.

2.4 Elastic Constitutive Equation

The incremental elastic constitutive equation is the generalized Hooke's Law relating the increment in Jaumann stress components and the elastic part (${}_t\Delta e_{ij}^e$) of the incremental Green-Lagrange strain components:

$${}_t\Delta \sigma_{ij} = C_{ijkl}^E {}_t\Delta e_{kl}^e \quad (2.6)$$

The tensor C_{ijkl}^E for isotropic case is given by:

$$C_{ijkl}^E = \lambda \delta_{ij} \delta_{kl} + 2\mu \delta_{ik} \delta_{jl} \quad (2.7)$$

where λ and μ are Lamé's constants.

2.5 Elasto-plastic Constitutive Equation

As the stresses in the material exceed the yield stress, the material undergoes plastic deformation. The elastic constitutive relation described above is not applicable for the plastic deformation. An elasto-plastic relationship between the incremental stress and strain tensors based on the von Mises yield criterion and isotropic hardening is developed below.

For an isotropically hardening material, the plastic potential is given by [1]¹:

$$F(\sigma_{ij}, p) = \sigma_{eq}(\sigma_{ij}) - \sigma_y(p) \quad (2.8)$$

where,

$$F = 0 \quad (2.9)$$

represents the yield criterion. The plastic potential F depends on the Cauchy stress tensor through the second invariant of its deviatoric part, called as equivalent stress, and defined by:

$$\sigma_{eq} = \left(\frac{3}{2} \sigma'_{ij} \sigma'_{ij} \right)^{\frac{1}{2}} \quad (2.10)$$

where σ'_{ij} is the deviatoric part of σ_{ij} . Further, F depends on the variable yield stress of the material, σ_y , through the hardening parameter p . Assuming that the strain hardening hypothesis is valid, p is the equivalent plastic strain ε_{eq}^p . Therefore,

$$p = \varepsilon_{eq}^p = \int d\varepsilon_{eq}^p \quad (2.11)$$

where,

$$d\varepsilon_{eq}^p = \left(\frac{2}{3} d\varepsilon_{ij}^p d\varepsilon_{ij}^p \right)^{\frac{1}{2}} \quad (2.12)$$

Here, $d\varepsilon_{ij}^p$ is the plastic part of the incremental linear strain tensor $d\varepsilon_{ij}$ and the integration in equation (2.11) is to be carried along the particle path. The dependence of σ_y on p is approximated by a power law type relationship:

$$\sigma_y - (\sigma_y)_0 = K(\varepsilon_{eq}^p)^n \quad (2.13)$$

Here, $(\sigma_y)_0$ is the yield stress at zero plastic strain, K is the hardening coefficient and n is called as the hardening exponent.

¹In this section, the superscript/subscript denoting time have been omitted for convenience

The plastic part of incremental linear strain tensor $d\varepsilon_{ij}^p$ is obtained from the plastic potential using the following relation:

$$d\varepsilon_{ij}^p = d\lambda \frac{\partial F}{\partial \sigma_{ij}} \quad (2.14)$$

where $d\lambda$ is a scalar. This equation is called as Flow Rule. Differentiation of equation (2.8) with respect to σ_{ij} gives:

$$\frac{\partial F}{\partial \sigma_{ij}} = \frac{3}{2\sigma_{eq}} \sigma'_{ij} \quad (2.15)$$

Therefore, $d\lambda$ is determined as:

$$d\lambda = d\varepsilon_{eq}^p \quad (2.16)$$

Further, the hardening relationship and the yield condition can be used to express $d\lambda$ as:

$$d\lambda = \frac{d\sigma_y}{H} = \frac{d\sigma_{eq}}{H} \quad (2.17)$$

where,

$$H = \frac{d\sigma_y}{d\varepsilon_{eq}^p} = Kn(\varepsilon_{eq}^p)^{n-1} \quad (2.18)$$

is the slope of the hardening curve. Substitution of equations (2.15) and (2.17) in equation (2.14) leads to the following constitutive equation:

$$d\varepsilon_{eq}^p = \frac{3}{2H\sigma_{eq}} \sigma'_{ij} d\sigma_{kl} \quad (2.19)$$

This constitutive relationship between the deviatoric stress tensor and the plastic part of the incremental linear strain tensor is not really convenient for the Updated Lagrangian formulation for which an incremental stress-strain relationship is needed. This can be obtained from equation (2.19) as follows:

$$d\varepsilon_{eq}^p = \frac{3\sigma'_{ij}}{2H\sigma_{eq}} \frac{\partial \sigma_{eq}}{\partial \sigma_{kl}} d\sigma_{kl} \quad (2.20)$$

Note that, from equations (2.8) and (2.15), we get:

$$\frac{\partial \sigma_{eq}}{\partial \sigma_{kl}} = \frac{\partial F}{\partial \sigma_{kl}} = \frac{3}{2\sigma_{eq}} \sigma'_{kl} \quad (2.21)$$

Substitution of equation (2.21) in equation (2.20) leads to the following incremental plastic stress-strain relationship:

$$d\varepsilon_{ij}^p = \frac{9}{4H\sigma_{eq}^2} \sigma'_{ij} \sigma'_{kl} d\sigma_{kl} \quad (2.22)$$

The incremental elastic stress-strain relationship (equations (2.6) & (2.7)) in terms of the incremental linear strain can be expressed as:

$$d\varepsilon_{ij}^e = \frac{1}{E} [-\nu d\sigma_{kk} \delta_{ij} + (1 + \nu) d\sigma_{ij}] \quad (2.23)$$

where, ε_{ij}^e is the elastic part of ε_{ij} , E is the Young's modulus and ν is the Poisson's ratio. Adding the two relationships, we get:

$$\varepsilon_{ij} = \varepsilon_{ij}^e + \varepsilon_{ij}^p = \left[\frac{-\nu}{E} \delta_{ij} \delta_{kl} + \frac{1+\nu}{E} \delta_{ik} \delta_{jl} + \frac{9}{4H} \frac{\sigma'_{ij} \sigma'_{kl}}{\sigma_{eq}^2} \right] d\sigma_{kl} \quad (2.24)$$

This is the incremental elasto-plastic stress-strain relationship needed in the updated Lagrangian formulation. However, it is the following inverse relationship which is more useful:

$$d\sigma_{ij} = C_{ijkl}^{EP} d\varepsilon_{kl} \quad (2.25)$$

where,

$$C_{ijkl}^{EP} = 2\mu \left(\delta_{ik} \delta_{jl} + \frac{\nu}{1-2\nu} \delta_{ij} \delta_{kl} - \frac{9\mu}{2(3\mu + H)} \frac{\sigma'_{ij} \sigma'_{kl}}{\sigma_{eq}^2} \right) \quad (2.26)$$

Here, μ is one of the Lamé's constants (also called as shear modulus) and ν is Poisson's ratio.

Note that the stress increment appearing in equation (2.26) must be an objective stress increment in the sense that $d\sigma_{ij}$ must be a zero tensor if the increment is a pure rotation. The incremental stress measure used in the present work is the Jaumann stress measure discussed in section 2.2.

The relationship (2.25) has been derived assuming the increment size to be small and using the incremental linear strain tensor as the strain measure. When a large size increment is to be used along with the incremental Green-Lagrange strain measure (defined in section (2.3)), the derivation is similar. The relationship (2.25), when the stress and strain measures are replaced respectively by the incremental objective stress measure and the incremental Green-Lagrange strain measure, takes the following form:

$${}_t\Delta\sigma_{ij} = \int_t^{t+\Delta t} {}^tC_{ijkl}^{EP} d({}_t\Delta e_{kl}) \quad (2.27)$$

where,

$${}^tC_{ijkl}^{EP} = 2\mu \left(\delta_{ik} \delta_{jl} + \frac{\nu}{1-2\nu} \delta_{ij} \delta_{kl} - \frac{9\mu}{2(3\mu + H)} \frac{{}^t\sigma'_{ij} {}^t\sigma'_{kl}}{({}^t\sigma_{eq}^p)^{n-1} {}^t\sigma_{eq}^2} \right) \quad (2.28)$$

Here, H has been replaced by the expression (2.18) and the left subscript t has been added to make it explicit that these quantities are to be evaluated at time t .

2.6 Incremental Updated Lagrangian Formulation

The objective of the updated Lagrangian formulation is to establish dynamic equilibrium in the configuration at time $t + \Delta t$ when all the static and kinematic variables at time t

are known. The principle of virtual work requires that [4]:

$$\int_{t+\Delta t V} {}^{t+\Delta t}\rho {}^{t+\Delta t}\ddot{u}_i \delta({}^{t+\Delta t}u_i) d{}^{t+\Delta t}V + \int_{t+\Delta t V} {}^{t+\Delta t}\sigma_{ij} \delta({}^{t+\Delta t}\varepsilon_{ij}) d{}^{t+\Delta t}V = {}^{t+\Delta t}R \quad (2.29)$$

where,

${}^{t+\Delta t}\rho$ = density at time $t + \Delta t$

${}^{t+\Delta t}\ddot{u}_i$ = acceleration at time $t + \Delta t$

$\delta({}^{t+\Delta t}u_i)$ = virtual displacement at time $t + \Delta t$

${}^{t+\Delta t}V$ = volume at time $t + \Delta t$

${}^{t+\Delta t}\sigma_{ij}$ = Cauchy stress tensor at $t + \Delta t$.

The virtual linear strain $\delta({}^{t+\Delta t}\varepsilon_{ij})$ is defined as:

$$\delta({}^{t+\Delta t}\varepsilon_{ij}) = \frac{1}{2} \left(\frac{\partial \delta({}^{t+\Delta t}u_i)}{\partial {}^{t+\Delta t}x_j} + \frac{\partial \delta({}^{t+\Delta t}u_j)}{\partial {}^{t+\Delta t}x_i} \right) \quad (2.30)$$

Further,

$$\begin{aligned} {}^{t+\Delta t}R = & \int_{t+\Delta t V} {}^{t+\Delta t}b_i \delta({}^{t+\Delta t}u_i) d{}^{t+\Delta t}V + \int_{t+\Delta t S_F} {}^{t+\Delta t}(t_i)_S \delta({}^{t+\Delta t}u_i) d{}^{t+\Delta t}S + \\ & \int_{t+\Delta t S_C} {}^{t+\Delta t}(t_i)_C \delta({}^{t+\Delta t}u_i) d{}^{t+\Delta t}S \end{aligned} \quad (2.31)$$

where,

${}^{t+\Delta t}b_i$ = body force per unit volume at time $t + \Delta t$

${}^{t+\Delta t}(t_i)_S$ = applied traction per unit area at time $t + \Delta t$

${}^{t+\Delta t}S_F$ = surface at time $t + \Delta t$ with traction specified

${}^{t+\Delta t}(t_i)_C$ = contact traction per unit area at time $t + \Delta t$

${}^{t+\Delta t}S_C$ = contact surface at time $t + \Delta t$

The main difficulty in applying equation (2.29) is that the configuration at time $t + \Delta t$ is unknown. Therefore, the virtual work expression at time $t + \Delta t$ is transformed to an integral over the volume at time t by using the principle conservation of mass. It is assumed that the external load term (2.31) is deformation independent for the formulation of governing equation. The expression (2.29) after the transformation becomes [4]:

$$\int_{{}_tV} {}^t\rho {}^{t+\Delta t}\ddot{u}_i \delta({}^{t+\Delta t}u_i) d{}^tV + \int_{{}_tV} {}^{t+\Delta t}{}_tS_{ij} \delta({}^{t+\Delta t}{}_te_{ij}) d{}^tV = {}^{t+\Delta t}R \quad (2.32)$$

where the virtual green-Lagrange strain tensor $\delta({}^{t+\Delta t}{}_te_{ij})$ is defined by:

$$\delta({}^{t+\Delta t}{}_te_{ij}) = \frac{1}{2} \left[\frac{\partial \delta({}^{t+\Delta t}u_i)}{\partial {}^{t+\Delta t}x_j} + \frac{\partial \delta({}^{t+\Delta t}u_j)}{\partial {}^{t+\Delta t}x_i} + \delta \left(\frac{\partial {}^{t+\Delta t}u_k}{\partial {}^{t+\Delta t}x_i} \frac{\partial {}^{t+\Delta t}u_k}{\partial {}^{t+\Delta t}x_j} \right) \right] \quad (2.33)$$

The second Piola-Kirchoff stress tensor can be decomposed as:

$${}^{t+\Delta t}S_{ij} = {}^tS_{ij} + {}_t\Delta S_{ij} = {}^t\sigma_{ij} + {}_t\Delta S_{ij} \quad (2.34)$$

Since,

$$\delta({}^{t+\Delta t}u_i) = \delta({}^tu_i + {}_t\Delta u_i) = \delta({}_t\Delta u_i) \quad (2.35)$$

the virtual Green-Lagrange strain tensor can be decomposed as:

$$\delta({}^{t+\Delta t}e_{ij}) = \delta({}_t\Delta e_{ij}) = \delta({}_t\Delta \varepsilon_{ij} + {}_t\Delta \eta_{ij}) \quad (2.36)$$

where,

$${}_t\Delta \varepsilon_{ij} = \frac{1}{2}({}_t\Delta u_{i,j} + {}_t\Delta u_{j,i}) \quad (2.37)$$

$${}_t\Delta \eta_{ij} = \frac{1}{2}({}_t\Delta u_{k,j} - {}_t\Delta u_{k,i}) \quad (2.38)$$

Therefore, the equation (2.32) can be written with incremental decomposition as:

$$\begin{aligned} \int_{{}_tV} {}^t\rho {}^{t+\Delta t}\ddot{u}_i \delta({}_t\Delta u_i) d{}^tV + \int_{{}_tV} {}_t\Delta S_{ij} \delta({}_t\Delta \varepsilon_{ij}) d{}^tV + \\ \int_{{}_tV} {}_t\Delta S_{ij} \delta({}_t\Delta \eta_{ij}) d{}^tV + \int_{{}_tV} {}^t\sigma_{ij} \delta({}_t\Delta \eta_{ij}) d{}^tV + \\ \int_{{}_tV} {}^t\sigma_{ij} \delta({}_t\Delta \varepsilon_{ij}) d{}^tV = {}^{t+\Delta t}R \end{aligned} \quad (2.39)$$

The above equation is simplified by neglecting the third integral, which is a higher order term, and approximating ${}_t\Delta S_{ij}$ as ${}^tC_{ijkl}^{EP} {}_t\Delta \varepsilon_{kl}$:

$$\begin{aligned} \int_{{}_tV} {}^t\rho {}^{t+\Delta t}\ddot{u}_i \delta({}_t\Delta u_i) d{}^tV + \int_{{}_tV} {}^tC_{ijkl}^{EP} {}_t\Delta \varepsilon_{kl} \delta({}_t\Delta \varepsilon_{ij}) d{}^tV + \\ \int_{{}_tV} {}^t\sigma_{ij} \delta({}_t\Delta \eta_{ij}) d{}^tV + \int_{{}_tV} {}^t\sigma_{ij} \delta({}_t\Delta \varepsilon_{ij}) d{}^tV = {}^{t+\Delta t}R \end{aligned} \quad (2.40)$$

The linearized equation, when solved, will yield only approximate displacement, velocity, acceleration, strain and stress fields. The approximate quantities are denoted by a right superscript (1). The error due to the approximation involved is calculated from equation (2.29) as:

$$\begin{aligned} Error = {}^{t+\Delta t}R - \int_{{}_t+\Delta tV^{(1)}} {}^{t+\Delta t}\sigma_{ij}^{(1)} \delta({}^{t+\Delta t}\varepsilon_{ij}^{(1)}) d{}^{t+\Delta t}V^{(1)} - \\ \int_{{}_t+\Delta tV^{(1)}} {}^{t+\Delta t}\rho^{(1)} {}^{t+\Delta t}\ddot{u}_i^{(1)} d{}^{t+\Delta t}V^{(1)} \end{aligned} \quad (2.41)$$

This error is generally minimised by a predictor – corrector scheme.

Chapter 3

Finite Element-Finite Difference Formulation

The mathematical formulation of the *Dynamic Elasto-plastic problem* is given in the equation (2.40) of chapter (2). However, this equation contains volume and surface integrals, which can not be solved analytically for most of the physical problems. In many of the cases of interest, the volume and surface may not be expressed mathematically. This necessitates the use of some numerical methods for the solution of the governing equation. Since it approximates the field variable and geometry simultaneously, the *Finite Element Method* is probably the most powerful method for solving the complex boundary value problems. The integration in the time domain, which is an initial value problem, is carried out efficiently using a *Finite Difference Scheme*. This chapter presents the development of a finite element – finite difference scheme for solving the linearized governing equation of the dynamic elasto-plastic problem. A numerical iterative technique for minimizing the error term given by equation (2.41) is also presented.

3.1 Matrix Notation

Matrix notation is used in the development of finite element – finite difference equations for the convenience in computer implementation.

The components of the strain tensors ${}_t\Delta\varepsilon_{ij}$ and ${}_t\Delta\eta_{ij}$ are represented in the array form as follows:

$${}_t\{\Delta\varepsilon\}^T = \{{}_t\Delta\varepsilon_{xx}, {}_t\Delta\varepsilon_{yy}, {}_t\Delta\varepsilon_{zz}, 2{}_t\Delta\varepsilon_{xy}, 2{}_t\Delta\varepsilon_{yz}, 2{}_t\Delta\varepsilon_{xz}\} \quad (3.1)$$

$${}^t\{\Delta\eta\}^T = \{{}^t\Delta u_{,x}, {}^t\Delta u_{,y}, {}^t\Delta u_{,z}, {}^t\Delta v_{,x}, \dots\} \quad (3.2)$$

Note that the shear strain components in the array ${}^t\{\Delta\varepsilon\}^T$ contain a factor of 2, which is a convention followed in most finite element formulations. The components of the Cauchy stress tensor ${}^t\sigma_{ij}$ are written as:

$${}^t\{\sigma\}^T = \{{}^t\sigma_{xx}, {}^t\sigma_{yy}, {}^t\sigma_{zz}, {}^t\sigma_{xy}, {}^t\sigma_{yz}, {}^t\sigma_{zx}\} \quad (3.3)$$

The matrix form of the fourth order tensor ${}^tC_{ijkl}^{EP}$ is given by:

$${}^t[C^{EP}] = \left([C^E] - \frac{[C^E] {}^t\{a\} {}^t\{a\}^T [C^E]}{{}^tA + {}^t\{a\}^T [C^E] {}^t\{a\}} \right) \quad (3.4)$$

where,

$${}^t\{a\} = \frac{3}{2 {}^t\sigma_{eq}} {}^t\{\sigma'\} \quad (3.5)$$

$${}^tA = K n {}^t(\varepsilon_{eq}^p)^{n-1} \quad (3.6)$$

The array ${}^t\{\sigma'\}^T$ represents the deviatoric part of the Cauchy stress at time t and ${}^t\varepsilon_{eq}^p$ stands for the equivalent plastic strain at time t . For an isotropic material, the matrix $[C^E]$ for the 3-D case is given by:

$$[C^E] = \frac{E}{(1+\nu)(1-2\nu)} \begin{bmatrix} 1-\nu & \nu & \nu & 0 & 0 & 0 \\ \nu & 1-\nu & \nu & 0 & 0 & 0 \\ \nu & \nu & 1-\nu & 0 & 0 & 0 \\ 0 & 0 & 0 & \frac{1-2\nu}{2} & 0 & 0 \\ 0 & 0 & 0 & 0 & \frac{1-2\nu}{2} & 0 \\ 0 & 0 & 0 & 0 & 0 & \frac{1-2\nu}{2} \end{bmatrix} \quad (3.7)$$

Equation (2.41) can be written in the following form owing to the symmetries of ${}^tC_{ijkl}^{EP}$, ${}^t\Delta\varepsilon_{ij}$, ${}^t\Delta\eta_{ij}$ and ${}^t\sigma_{ij}$:

$$\begin{aligned} & \int_{{}^tV} \delta({}^t\{\Delta u\}^T) {}^t\rho {}^{t+\Delta t}\{\ddot{u}\} d{}^tV + \int_{{}^tV} \delta({}^t\{\Delta\varepsilon\}^T) {}^t[C^{EP}] {}^t\{\Delta\varepsilon\} d{}^tV \\ & + \int_{{}^tV} \delta({}^t\{\Delta\eta\}^T) {}^t[T] {}^t\{\Delta\eta\} d{}^tV + \int_{{}^tV} \delta({}^t\{\Delta\varepsilon\}^T) {}^t\{\sigma\} d{}^tV = {}^{t+\Delta t}R \end{aligned} \quad (3.8)$$

The matrix $[T]$ is given by:

$${}^t[T] = \begin{bmatrix} {}^t[\Sigma] & 0 & 0 \\ 0 & {}^t[\Sigma] & 0 \\ 0 & 0 & {}^t[\Sigma] \end{bmatrix} \quad (3.9)$$

where,

$${}^t[\Sigma] = \begin{bmatrix} {}^t\sigma_{xx} & {}^t\sigma_{xy} & {}^t\sigma_{xz} \\ {}^t\sigma_{xy} & {}^t\sigma_{yy} & {}^t\sigma_{yz} \\ {}^t\sigma_{xz} & {}^t\sigma_{yz} & {}^t\sigma_{zz} \end{bmatrix} \quad (3.10)$$

3.2 Finite Element Formulation

The domain is discretized into a number of elements and the incremental displacement field is approximated over each element by:

$${}^t\{\Delta u\} = \begin{Bmatrix} {}^t\Delta u \\ {}^t\Delta v \\ {}^t\Delta w \end{Bmatrix} = {}^t[\Phi] {}^t\{\Delta u\}^e \quad (3.11)$$

Here, the element incremental displacement vector is given by:

$${}^t\{\Delta u\}^e = \{{}^t\Delta u^1, {}^t\Delta v^1, {}^t\Delta w^1, {}^t\Delta u^2, \dots\} \quad (3.12)$$

where the quantities ${}^t\Delta u^i$, ${}^t\Delta v^i$, ${}^t\Delta w^i$ stand for the unknown incremental displacements of node i in x , y and z directions respectively. The matrix ${}^t[\Phi]$ is defined by:

$${}^t[\Phi] = \begin{bmatrix} {}^t\{\Phi_1\}^T \\ {}^t\{\Phi_2\}^T \\ \vdots \\ {}^t\{\Phi_1\}^T \end{bmatrix} \quad (3.13)$$

where,

$$\begin{aligned} {}^t\{\Phi_1\}^T &= \{{}^tN_1, 0, 0, {}^tN_2, 0, 0, \dots\} \\ {}^t\{\Phi_2\}^T &= \{0, {}^tN_1, 0, 0, {}^tN_2, 0, \dots\} \\ {}^t\{\Phi_3\}^T &= \{0, 0, {}^tN_1, 0, 0, {}^tN_2, \dots\} \end{aligned} \quad (3.14)$$

The tN_i , which are functions of (x, y, z) , are called as shape functions. In the present work, 8-noded brick element with trilinear shape functions is used. The functions tN_i do not depend explicitly on t . However, the left superscript t is used to emphasize the fact that the shape of element (nodal coordinates) changes with time.

The acceleration can similarly be expressed as:

$${}^{t+\Delta t}\{\ddot{u}\} = \begin{Bmatrix} {}^{t+\Delta t}\ddot{u}_i \\ {}^{t+\Delta t}\ddot{v}_j \\ {}^{t+\Delta t}\ddot{w}_k \end{Bmatrix} = {}^t[\phi] {}^{t+\Delta t}\{\ddot{u}\}^e \quad (3.15)$$

The strain field is expressed in terms of the nodal displacements by differentiating (3.11) and using the expressions (2.37) and (2.38) as:

$${}^t\{\Delta\varepsilon\} = {}^t[B_L] {}^t\{\Delta u\}^e \quad (3.16)$$

$${}^t\{\Delta\eta\} = {}^t[B_N] {}^t\{\Delta u\}^e \quad (3.17)$$

where,

$${}^t[B_L] = \begin{bmatrix} {}^t\{\Phi_1\}_{,x}^T \\ {}^t\{\Phi_2\}_{,y}^T \\ {}^t\{\Phi_3\}_{,z}^T \\ {}^t\{\Phi_2\}_{,x}^T + {}^t\{\Phi_1\}_{,y}^T \\ {}^t\{\Phi_3\}_{,y}^T + {}^t\{\Phi_2\}_{,z}^T \\ {}^t\{\Phi_1\}_{,z}^T + {}^t\{\Phi_3\}_{,x}^T \end{bmatrix} \quad (3.18)$$

and

$${}^t[B_N]^T = \left\{ {}^t\{\Phi_1\}_{,x}, {}^t\{\Phi_1\}_{,y}, {}^t\{\Phi_1\}_{,z}, {}^t\{\Phi_2\}_{,x}, \dots \right\} \quad (3.19)$$

Using the equations (3.11), (3.15), (3.16) and (3.17), the contribution to the integral (3.8) over a typical element with volume V^e is:

$$\begin{aligned} & \delta({}^t\{\Delta u\}^{eT}) \left(\int_{V^e} {}^t[\Phi]^T {}^t\rho {}^t[\Phi] dV^e \right) {}^{t+\Delta t}\{\ddot{u}\}^e + \\ & \delta({}^t\{\Delta u\}^{eT}) \left(\int_{V^e} {}^t[B_L]^T {}^t[C^{EP}] {}^t[B_L] dV^e \right) {}^t\{\Delta u\}^e + \\ & \delta({}^t\{\Delta u\}^{eT}) \left(\int_{V^e} {}^t[B_N]^T {}^t[T] {}^t[B_N] dV^e \right) {}^t\{\Delta u\}^e + \\ & \delta({}^t\{\Delta u\}^{eT}) \left(\int_{V^e} {}^t[B_L]^T {}^t\{\sigma\} dV^e \right) = \delta({}^t\{\Delta u\}^{eT}) {}^{t+\Delta t}\{F\}^e \end{aligned} \quad (3.20)$$

The contribution to the term ${}^{t+\Delta t}\mathcal{R}$ is expressed in terms of the elemental external force vector ${}^{t+\Delta t}\{F\}^e$ using a standard procedure [48].

Since the variation in the displacement vector is arbitrary, the above equation can be written as:

$${}^t[M]^e {}^{t+\Delta t}\{\ddot{u}\}^e + {}^t[K]^e {}^t\{\Delta u\}^e + {}^t\{f\}^e = {}^{t+\Delta t}\{F\}^e \quad (3.21)$$

where the element mass matrix ${}^t[M]^e$ is defined as:

$${}^t[M]^e = \int_{V^e} {}^t[\Phi]^T {}^t\rho {}^t[\Phi] dV^e \quad (3.22)$$

and the elemental stiffness matrix ${}^t[K]^e$ is expressed as:

$${}^t[K]^e = {}^t[K_L]^e + {}^t[K_{NL}]^e \quad (3.23)$$

where,

$${}^t[K_L]^e = \int_{{}^tV^e} {}^t[B_L]^T {}^t[C^{EP}] {}^t[B_L] d{}^tV^e \quad (3.24)$$

$${}^t[K_{NL}]^e = \int_{{}^tV^e} {}^t[B_N]^T {}^t[T] {}^t[B_N] d{}^tV^e \quad (3.25)$$

The elemental internal force vector is:

$${}^t\{f\}^e = \int_{{}^tV^e} {}^t[B_L]^T {}^t\{\sigma\} d{}^tV^e \quad (3.26)$$

The element mass (${}^t[M]^e$) and stiffness (${}^t[K]^e$) matrices along with the element force vectors ${}^t\{f\}^e$ and ${}^{t+\Delta t}\{F\}^e$ are assembled to obtain the global equation:

$${}^t[M] {}^{t+\Delta t}\{\ddot{U}\} + {}^t[K] {}^t\{\Delta U\} + {}^t\{f\} = {}^{t+\Delta t}\{F\} \quad (3.27)$$

where,

${}^t[M]$ = global mass matrix

${}^t[K]$ = global stiffness matrix

${}^t\{f\}$ = global internal force vector at time t

${}^{t+\Delta t}\{F\}$ = global external force vector at $t + \Delta t$.

The equation (3.27) represents a system of ordinary coupled second order linear differential equations. The next section describes the technique to convert it into a system of algebraic equations.

3.3 Finite Difference Scheme

The number of efficient methods for the solution of a large system of coupled ordinary differential equations such as those arising from a finite element formulation is limited. A popular technique is the direct integration of equation (3.27), where the dynamic equilibrium is sought only at discrete time intervals instead of at all times t . The assumptions on the variations of displacement, velocity and acceleration within each time interval determine the accuracy, stability and cost of the solution procedure.

Two broad classifications exist in the direct integration methods: *Explicit* and *Implicit integration methods*. Explicit integration methods use the equilibrium conditions at time t for obtaining the solution at time $t + \Delta t$ and hence these procedures are only conditionally stable. One main advantage of explicit schemes is that factorization of the effective stiffness matrix is not necessary. Implicit integration methods use the dynamic equilibrium

conditions at both time t and $t + \Delta t$ for obtaining the solution at time $t + \Delta t$. Since the implicit time integration methods are unconditionally stable, the time step used can be several orders of magnitudes larger, but the factorization of effective stiffness matrix is necessary for obtaining the solution. In this work, an implicit method called *Newmark method* is used for integration.

The Newmark method makes use of the following assumptions [4]:

$$\begin{aligned} {}^{t+\Delta t}\{\dot{U}\} &= {}^t\{\dot{U}\} + \left[(1 - \delta) {}^t\{\ddot{U}\} + \delta {}^{t+\Delta t}\{\ddot{U}\} \right] \Delta t \\ {}^{t+\Delta t}\{U\} &= {}^t\{U\} + {}^t\{\dot{U}\} \Delta t + \left[\left(\frac{1}{2} - \alpha \right) {}^t\{\ddot{U}\} + \alpha {}^{t+\Delta t}\{\ddot{U}\} \right] (\Delta t)^2 \end{aligned} \quad (3.28)$$

The parameters α and δ can be determined so as to obtain desired accuracy and stability. The constant average acceleration method corresponding to $\alpha = \frac{1}{4}$ and $\delta = \frac{1}{2}$ is used in this work, which results in an implicit unconditionally stable integration scheme.

The Newmark constants are defined below:

$$\begin{aligned} a_0 &= \frac{1}{\alpha(\Delta t)^2} \\ a_1 &= \frac{1}{\alpha(\Delta t)} \\ a_2 &= \frac{1}{2\alpha} - 1 \\ a_3 &= \Delta t(1 - \delta) \\ a_4 &= \delta \Delta t \end{aligned} \quad (3.29)$$

Substituting for ${}^{t+\Delta t}\{\ddot{U}\}$ from equation (3.28) and splitting ${}^{t+\Delta t}\{U\}$ as:

$${}^{t+\Delta t}\{U\} = {}^t\{U\} + {}^t\{\Delta U\} \quad (3.30)$$

the expression (3.27) becomes:

$${}^t[K_d] {}^t\{\Delta U\} + (a_0 {}^t[M] {}^t\{U\} + {}^t\{f\}) = {}^{t+\Delta t}\{F_d\} \quad (3.31)$$

where the effective stiffness matrix ${}^t[K_d]$ and the effective force vector ${}^{t+\Delta t}\{F_d\}$ are given by:

$${}^t[K_d] = a_0 {}^t[M] + {}^t[K] \quad (3.32)$$

$${}^{t+\Delta t}\{F_d\} = {}^{t+\Delta t}\{F\} + {}^t[M](a_0 {}^t\{U\} + a_1 {}^t\{\dot{U}\} + a_2 {}^t\{\ddot{U}\}) \quad (3.33)$$

Since the dynamic equilibrium is satisfied at time t and assuming that changes in mass matrix in an increment is not very significant, the following equation must hold, which

can be obtained from the finite element discretization of the integral (2.29) written at time t :

$${}^t[M] {}^t\{\ddot{U}\} + {}^t\{f\} = {}^t\{F\} \quad (3.34)$$

Using equation (3.28), this can be expressed as:

$$a_0 {}^t[M] {}^t\{U\} + {}^t\{f\} = {}^t\{F_d\} \quad (3.35)$$

Decomposing the effective force vector as:

$${}^{t+\Delta t}\{F_d\} = {}^t\{F_d\} + {}_t\{\Delta F_d\} \quad (3.36)$$

and using the expression (3.35) for ${}^t\{F_d\}$, the following equation in ${}_t\{\Delta U\}$ is obtained from equation (3.31):

$${}^t[K_d] {}_t\{\Delta U\} = {}_t\{\Delta F_d\} \quad (3.37)$$

Using equations (3.33) and (3.35) we get:

$${}_t\{\Delta F_d\} = {}^{t+\Delta t}\{F_d\} - {}^t\{F_d\} = {}^{t+\Delta t}\{F\} - {}^t\{f\} + {}^t[M](a_1 {}^t\{\dot{U}\} + a_2 {}^t\{\ddot{U}\}) \quad (3.38)$$

This algebraic equation system is solved to obtain the incremental displacement vector ${}_t\{\Delta U\}$.

Once the incremental displacement is obtained by solving equation (3.37), the velocity and acceleration at time $t + \Delta t$ are obtained using the following expressions:

$${}^{t+\Delta t}\{\ddot{U}\} = a_0 ({}^{t+\Delta t}\{U\} - {}^t\{U\}) - a_1 {}^t\{\dot{U}\} - a_2 {}^t\{\ddot{U}\} \quad (3.39)$$

$${}^{t+\Delta t}\{\dot{U}\} = {}^t\{\dot{U}\} + a_3 {}^t\{\ddot{U}\} + a_4 {}^{t+\Delta t}\{\ddot{U}\} \quad (3.40)$$

3.4 Determination of Stress

The evaluation of stress components (at the Gauss points) is done by the following procedure:

1. The linear and non-linear strains are obtained by:

$${}_t\{\Delta \varepsilon\} = {}^t[B_L] {}_t\{\Delta u\}^e \quad (3.41)$$

$${}_t\{\Delta \eta\} = {}^t[B_N] {}_t\{\Delta u\}^e \quad (3.42)$$

2. The Green-Lagrange strain is obtained by combining the linear and non-linear parts using equations (2.5), (3.1) and (3.2) in equation (2.4).

3. From the Green-Lagrange strain; the Jaumann stress increment is found using the procedure described in section 3.4.1.
4. Finally, the Cauchy stress increment is calculated from the Jaumann stress increment using equations (2.2) and (2.3). This is added to the Cauchy stress at time t to find the Cauchy stress at time $t + \Delta t$.

3.4.1 Integration of the Constitutive Equation

Various techniques exist for the integration of the constitutive equation. A simple and robust technique is the *Euler forward integration* scheme discussed below.

Suppose that the state of the Gauss point at time t (*elastic or plastic*) is known.

- If the state at time t is *elastic*,
 1. Calculate the Jaumann stress increment assuming elastic behaviour.
 2. Determine the Cauchy stress increments using equations (2.2) & (2.3) and add it to Cauchy stress at time t , ${}^t\{\sigma\}$, to get the the Cauchy stress at time $t + \Delta t$, viz., ${}^{t+\Delta t}\{\sigma\}$.
 3. Determine ${}^t\sigma_{eq}$ and ${}^{t+\Delta t}\sigma_{eq}$ using equation (2.10).
 4. If ${}^{t+\Delta t}\sigma_{eq} \leq {}^t\sigma_y$, then the material point is still in elastic state. RETURN.

Else, a transition from elastic to plastic has occurred. Calculate:

$$Ratio = \frac{{}^{t+\Delta t}\sigma_{eq} - {}^t\sigma_y}{{}^{t+\Delta t}\sigma_{eq} - {}^t\sigma_{eq}} \quad (3.43)$$

and change the state to *plastic*. The sub-incrementation method is followed and the Jaumann stress increment is updated after each sub-increment by the change in stress components corresponding to the elasto-plastic strain sub-increment. Thus, the Jaumann stress increment is given by the relation:

$${}^t\{\overset{\circ}{\sigma} \Delta t\} = [C^E](1 - Ratio) {}^t\{\Delta e\} + \sum_{i=1}^n {}^{t+\Delta t}[C^{EP}]^{i-1} (Ratio/n) {}^t\{\Delta e\} \quad (3.44)$$

where the matrix ${}^{t+\Delta t}[C^{EP}]^{i-1}$ corresponds to $(i - 1)^{th}$ updated state.

- If the state at time t is *plastic*, check for unloading as described in section (3.4.2). If there is no unloading, the sub-incrementation method described in (4) above is applied with *Ratio* set to unity.

3.4.2 Unloading Scheme

The phenomenon of local unloading is to be incorporated to reproduce more closely the elasto-plastic response of a structure. The unloading criterion defined by Chakrabarty [8]:

$${}^t\{n\}^T {}^t\{\Delta e\} < 0 \quad (3.45)$$

where, ${}^t\{n\}^T$ represents the unit outward normal to the yield surface at the current stress point ${}^t\sigma$ in a 9-D stress space, is implemented in this work. Neutral loading and postive loading are represented by replacing the “<”symbol in (3.45) by “=” and “>” symbols respectively.

When unloading is detected, the yield stress at that Gauss point is changed to the equivalent stress at the Gauss point at time t (${}^t\sigma_y = {}^t\sigma_{eq}$), the state tag of the Gauss point is changed from plastic to elastic and the elastic constitutive equation is applied to calculate the incremental stress.

3.5 Skyline Scheme of Global Assembly

The three-dimensional dynamic elasto-plastic contact problem is computationally intensive one and therefore every effort should be made to reduce the storage and the computational time required for solving the problem. Skyline assembly scheme [4] is one such technique, which significantly reduces the storage required for the global stiffness matrix ${}^t[K]$. In this storage scheme, only the elements below the skyline of the matrix ${}^t[K]$ are stored in a one-dimensional array ${}^t\{A\}$. However, along with the storage scheme a specific procedure for addressing the elements of ${}^t[K]$ in ${}^t\{A\}$ is needed. Thus, before proceeding with the assembly of the element stiffness matrices it is necessary to establish the address of the global stiffness matrix elements in one-dimensional array ${}^t\{A\}$.

The element pattern of a typical global stiffness matrix is shown below:

$${}^t[K] = \begin{bmatrix} k_{11} & k_{12} & 0 & k_{14} & 0 \\ k_{12} & k_{22} & k_{23} & 0 & 0 \\ 0 & k_{23} & k_{33} & k_{34} & 0 \\ k_{14} & 0 & k_{34} & k_{44} & k_{45} \\ 0 & 0 & 0 & k_{45} & k_{55} \end{bmatrix}$$

Since the matrix ${}^t[K]$ is symmetric, only the elements above the diagonal and the diagonal elements need to be stored. Defining by m_i the row number of the first non-zero element

in column i , the variables $m_i = 1, \dots, n$ represent the skyline of the matrix, and the value $(m_{i+1} - m_i)$ represent the column height. (The zero elements below the skyline are stored, since they may become non-zero during the solution process). The column heights are determined from the connectivity arrays of the elements. Once the column heights of the global stiffness matrix are known, we can store all the elements below the skyline of ${}^t[K]$ as a one-dimensional array in ${}^t\{A\}$; i.e., the *active elements* (elements below the skyline) of ${}^t[K]$ are stored consecutively in ${}^t\{A\}$:

$${}^t\{A\}^T = \{k_{11}, k_{22}, k_{12}, k_{33}, k_{23}, k_{44}, k_{34}, 0, k_{14}, k_{55}, k_{45}\}$$

In addition to ${}^t\{A\}$, we also define an array $\{MAXA\}$, which stores the addresses of diagonal elements of ${}^t[K]$ in ${}^t\{A\}$; i.e., the address of the i^{th} diagonal element of ${}^t[K]$, k_{ii} , in array ${}^t\{A\}$ is given by $MAXA_i$. Thus,

$$\{MAXA\}^T = \{1, 2, 4, 6, 10, 12\}$$

Note that, $MAXA_i$ is equal to the sum of column heights upto the $(i-1)^{th}$ column plus 1. Hence the number of active elements in the i^{th} column of ${}^t[K]$ is equal to $MAXA_{i+1} - MAXA_i$, and the element addresses are $MAXA_i, (MAXA_i + 1), \dots, (MAXA_{i+1} - 1)$. It follows that using the above storage scheme of ${}^t[K]$ in ${}^t\{A\}$, together with the address array $\{MAXA\}$ as defined above, each element of ${}^t[K]$ in ${}^t\{A\}$ can be addressed easily.

3.6 Static Condensation Scheme

The contact analysis is done in an iterative manner to determine the nodes which are out of contact, in sticking contact or in slipping contact. Solving the complete system of equations in each iteration is highly inefficient in terms of time and computer resources, especially when the contact region is small compared to the whole system. In order to reduce the solution time, it is desirable to condense the effective stiffness matrix and the effective force vector to the size of the degrees of freedom to which the contact boundary conditions are to be applied.

The condensation procedure starts by dividing the nodes into two categories: the nodes at which the contact boundary conditions are to be applied (referred as the nodes of *type 1*) and the remaining nodes (referred as the nodes of *type 2*). To facilitate the condensation, the nodes are renumbered so that the nodes of type 1 are numbered first (called *internal*

node numbers, while the original node numbers are called *external node numbers*). Then the essential boundary conditions (i.e., the displacement boundary conditions) are applied to equation (3.37).

Then these equations are partitioned as follows:¹

$$\begin{bmatrix} [K_{11}] & [K_{12}] \\ [K_{21}] & [K_{22}] \end{bmatrix} \begin{Bmatrix} \{\Delta U_1\} \\ \{\Delta U_2\} \end{Bmatrix} = \begin{Bmatrix} \{\Delta F_1\} \\ \{\Delta F_2\} \end{Bmatrix} \quad (3.46)$$

where $\{\Delta U_1\}$ denotes the incremental displacement vector corresponding to the nodes of type 1 and $\{\Delta U_2\}$ denotes the incremental displacement vector corresponding to the nodes of type 2. Equation (3.46) can be separated as follows:

$$[K_{11}] \{\Delta U_1\} + [K_{12}] \{\Delta U_2\} = \{\Delta F_1\} \quad (3.47)$$

$$[K_{21}] \{\Delta U_1\} + [K_{22}] \{\Delta U_2\} = \{\Delta F_2\} \quad (3.48)$$

Solving for $\{\Delta U_2\}$ from equation (3.48), we get:

$$\{\Delta U_2\} = [K_{22}]^{-1} (\{\Delta F_2\} - [K_{21}] \{\Delta U_1\}) \quad (3.49)$$

Substitution of this expression for $\{\Delta U_2\}$ in equation (3.47) and rearrangement of the resulting equation leads to the following condensed set of dynamic equilibrium equations:

$$[\widehat{K}] \{\Delta \widehat{U}\} = \{\Delta \widehat{F}\} \quad (3.50)$$

where,

$$[\widehat{K}] = [K_{11}] - [K_{12}] [A] \quad (3.51)$$

$$\{\Delta \widehat{U}\} = \{\Delta U_1\} \quad (3.52)$$

$$\{\Delta \widehat{F}\} = \{\Delta F_1\} - [K_{12}] \{B\} \quad (3.53)$$

$$[A] = [K_{22}]^{-1} [K_{21}] \quad (3.54)$$

$$\{B\} = [K_{22}]^{-1} \{\Delta F_2\} \quad (3.55)$$

The number of equations in the condensed set (3.50) is equal to the number of degrees of freedom of type 1. The coefficient matrix $[\widehat{K}]$ and the right side vector $\{\Delta \widehat{F}\}$ are evaluated from equations (3.51 – 3.55) using the partitioned matrices and vectors of equation (3.46). Note that while evaluating $[A]$ and $\{B\}$, it is not necessary to invert the

¹In this section, the superscript/subscript denoting time have been omitted for the sake of convenience

matrix $[K_{22}]^{-1}$. Instead one can solve the following equations by the Gauss elimination method:

$$[K_{22}][A] = [K_{21}] \quad (3.56)$$

$$[K_{22}]\{B\} = \{\Delta F_2\} \quad (3.57)$$

To reduce the time further, one can store the upper triangular form of $[K_{22}]$. In this way, one can solve for the columns of $[A]$ by performing Gauss elimination and back substitution operations on the corresponding columns of $[K_{21}]$. The vector $\{B\}$ is obtained in similar fashion by performing the Gauss elimination and back substitution on the vector $\{\Delta F_2\}$.

3.7 Modified Newton-Raphson Scheme

The solution to equation (3.37) represents only an approximate solution to the governing equation (2.40), because of the linearization and simplifications employed in deriving the equation (3.37). The error obtained should to be minimized and there are various iterative techniques for this. One of the simplest and very effective technique is the *Modified Newton-Raphson algorithm*, which offers fast convergence with less computation [4].

This technique can elegantly be represented as follows:

Solve:

$${}^t[K_d] {}^t\{\Delta U\}^{(i)} = {}^t\{\Delta F_u\}^{(i-1)} \quad (3.58)$$

where,

$${}^t\{\Delta F_u\}^{(i-1)} = {}^{t+\Delta t}\{F\}^{(i-1)} - {}^{t+\Delta t}\{f\}^{(i-1)} - {}^{t+\Delta t}[M] {}^{t+\Delta t}\{\ddot{U}\}^{(i-1)} \quad (3.59)$$

$${}^t\{\Delta F_u\}^{(0)} = {}^t\{\Delta F_d\} \quad (3.60)$$

till the convergence criterion:

$$\frac{\|{}^t\{\Delta F_u\}^{(i)}\|}{\|{}^{t+\Delta t}\{F\}^{(i)}\|} \leq tol_c \quad (3.61)$$

is satisfied. The vector ${}^t\{\Delta F_u\}$ is called the *unbalance force vector*.

3.8 Divergence Handling Procedures

The modified Newton Raphson method diverges in some cases; i.e., the ratio of unbalance force to the external force, instead of reducing, increases in each iteration. Also, in

some other cases, the rate of convergence is not fast enough, requiring a large number of iterations for reducing the unbalance force to acceptable limits. Two of the methods, which are simple and fairly effective for handling divergence or accelerating the rate of convergence are *Under-relaxation method* and *Line search method* [7]. These methods are generally applied by modifying the displacement vector $_t\{\Delta u\}^{(i)}$. However, in the contact analysis scenario, it is not acceptable, since the contact status may get changed due to modification in the displacement vector. Therefore, in this work, these methods are applied by modifying the unbalance force vector $_t\{\Delta F_u\}^{(i-1)}$ and repeating the solution process when divergence is detected.

In this work, the Newton Raphson iterations are said to be diverging when:

$$\frac{\|_t\{\Delta F_u\}^{(i)}\|}{\|_t+\Delta t\{F\}^{(i)}\|} > \beta \frac{\|_t\{\Delta F_u\}^{(i-1)}\|}{\|_t+\Delta t\{F\}^{(i-1)}\|} \quad (3.62)$$

is satisfied. The value of the factor β is taken as 0.9.

The under-relaxation and line search methods are discussed below:

Under-relaxation method: If divergence is detected in the i^{th} iteration, the unbalance force vector $_t\{\Delta F_u\}^{(i-1)}$ is scaled by a factor α repeatedly, till the above criterion is not satisfied:

$$_t\{\Delta F_u\}^{(i-1)} = \alpha _t\{\Delta F_u\}^{(i-1)} \quad (3.63)$$

If the under-relaxation is not able to find a value of unbalance force for which the above criterion is not satisfied, the solution run is terminated with a warning message.

Line search method: In this method, the basic aim is to search for the point, which corresponds to minimum unbalance, along a direction specified by the unbalance force vector $_t\{\Delta F_u\}^{(i-1)}$. However, it is not very efficient to perform a full line search, since, in that case the number of solution runs required may become prohibitively high. The approach used is to repeat the solutions for a fixed number of values of factor α_j (defined below), within a preselected range.

$$_t\{\Delta F_u\}^{(i-1)} = \alpha_j _t\{\Delta F_u\}^{(i-1)} \quad (3.64)$$

$$\text{where, } \alpha_{min} \leq \alpha_j \leq \alpha_{max}$$

The value of α_j corresponding to the minimum unbalance force is chosen as the best point and the solution corresponding to this α_j is accepted as the result of line search method.

Since in both the above methods, the complete iteration is repeated, including a number of contact iterations, it is very costly to do either under-relaxation or line search, in terms of both computational time and resources. Therefore, it is preferable to use these methods only when some difficulties in convergence are observed. Under-relaxation is cheaper compared to line search, while line search is more efficient.

3.9 Numerical Aspects

The selection of parameters controlling the numerical scheme in dynamic non-linear analysis is of importance not only for efficiently obtaining the solution, but also for the accuracy of the solution. The following sections discuss various aspects related to the numerical scheme used.

3.9.1 Choice of Time-step

A procedure for the selection of time step is given in Bathe [4], which may be used to select an initial time step and mesh. A time step and mesh convergence study should then be performed to arrive at the proper values. It is important to note that an unconditionally stable method *does not* provide a solution close to the exact solution for an arbitrary time step. Phenomena such as amplitude reduction and period elongation may occur due to an improper choice of time step. Hence the proper way to perform a dynamic non-linear analysis is to study the effect of time step and mesh size on the solution and to search appropriate values.

The choice of a time step is based on the type of problem considered. In general, dynamic problems can be categorized as: 1. *Structural dynamics problems* and 2. *Wave propagation problems*.

Structural Dynamics Problem: The step by step procedure for modeling a structural dynamics problem is given below.

1. Identify the frequencies involved in loading, using a Fourier analysis if necessary. These frequencies may change with time. Let the highest significant frequency contained in the loading be w_u .

2. Choose a finite element mesh that can accurately represent the static response and accurately represent all frequencies upto about $w_{co} = 4w_u$, where w_{co} is called as the *optimum critical frequency*.
3. Perform the direct integration analysis. The time step Δt for this solution should be equal to about $\frac{1}{20}T_{co}$, where $T_{co} = \frac{2\pi}{w_{co}}$.

Wave Propagation Problems: Assuming that the critical wavelength to be calculated correctly is L_w , then the time taken by the wave to travel past a point is given by:

$$t_w = \frac{L_w}{c} \quad (3.65)$$

where c is the wave speed. Assuming that n time steps are necessary to represent the travel of the wave, the time step should be:

$$\Delta t = \frac{t_w}{n} \quad (3.66)$$

and the *effective length*² of a finite element should be:

$$L_e = c\Delta t \quad (3.67)$$

The above choice of time step and corresponding effective length represents the complete wave travel accurately. But, care has to be taken to ensure that $\Delta t \leq \frac{T_n}{\pi}$, where T_n is the smallest time period of the problem.

It is found that the most accurate solution is obtained by integrating with a time step equal to the above limits (denoted by Δt_{cr}) and the solution is less accurate, when a smaller time step is employed. This deterioration in the accuracy of the predicted solution when Δt is smaller than Δt_{cr} is more pronounced, when a relatively coarse spatial discretization is used.

3.9.2 Deformation Dependent Loading

Deformation dependent loading is taken care of by evaluating the consistent force vector ${}^{t+\Delta t}\{F\}$ at time $t + \Delta t$ for the calculation of the unbalance force vector (3.59). An alternate procedure given by Bathe *et al.* [11] incorporates deformation dependency into the formulation of the governing equation, but this results in an asymmetric stiffness matrix, the solution of which is computationally expensive. The method used in this work

²Effective length is the smallest distance between any two nodes in the mesh used

may take a slightly more number of iterations for convergence, but this loss is offset by the gains acquired by retaining a symmetric stiffness matrix.

3.9.3 Stress Updation

There exist two methods for updating the stress at a Gauss point: 1. *Iterative updation* and 2. *Incremental updation* (Crisfield [7]).

Iterative Updation: The iterative displacement is used to compute the iterative strain, which is then used in the constitutive equation to update the stress at iteration $(i-1)$ to stress at iteration (i) .

Incremental Updation: All the iterative displacements upto iteration (i) are added to find the cumulative incremental displacement of the current increment. This is used to compute the incremental strain, which is used in the constitutive equation to update the stress from last equilibrium point (end of the previous increment) to the state after iteration (i) .

The first method may lead to spurious unloading, since the unbalance force vector calculated in some iterations may be in different directions compared to that of the initial force vector. This can be avoided by using the incremental updation procedure.

Chapter 4

Contact Formulation

The dynamic, large deformation, elasto-plastic, updated Lagrangian finite element formulation developed in the last two chapters, can be used for contact analysis with appropriate modifications. The most important modification is the development of an additional set of finite element equations (involving the contact stiffness matrix) relating the unknown contact forces and displacements. These equations, which consist of the kinematic constraints and the contact force expressions based on the discretization of the contact boundary, are developed using the *Lagrange multiplier method*. These developments are described in the following sections. Finally the algorithm for the analysis of dynamic, large deformation, elasto-plastic contact including the effects of friction, is described.

4.1 Contact Constraints

A typical two body contact system is shown in figure (4.1). The bodies occupy the domains ${}^{t+\Delta t}\bar{V}^1$ and ${}^{t+\Delta t}\bar{V}^2$ at time $t + \Delta t$. The boundaries of ${}^{t+\Delta t}\bar{V}^1$ and ${}^{t+\Delta t}\bar{V}^2$ are denoted by ${}^{t+\Delta t}S^1$ and ${}^{t+\Delta t}S^2$ and their interior volumes by ${}^{t+\Delta t}V^1$ and ${}^{t+\Delta t}V^2$ respectively. At any time $t + \Delta t$, the boundary of contact body n ($n = 1, 2$) can be partitioned as:

$${}^{t+\Delta t}S^n = {}^{t+\Delta t}S_D^n \cup {}^{t+\Delta t}S_F^n \cup {}^{t+\Delta t}S_C^n \quad (4.1)$$

where,

${}^{t+\Delta t}S_D$ = surface on which displacements are specified,

${}^{t+\Delta t}S_F$ = surface on which tractions are specified,

${}^{t+\Delta t}S_C$ = surface on which contact occurs. Assuming the boundary ${}^{t+\Delta t}S^n$ to be

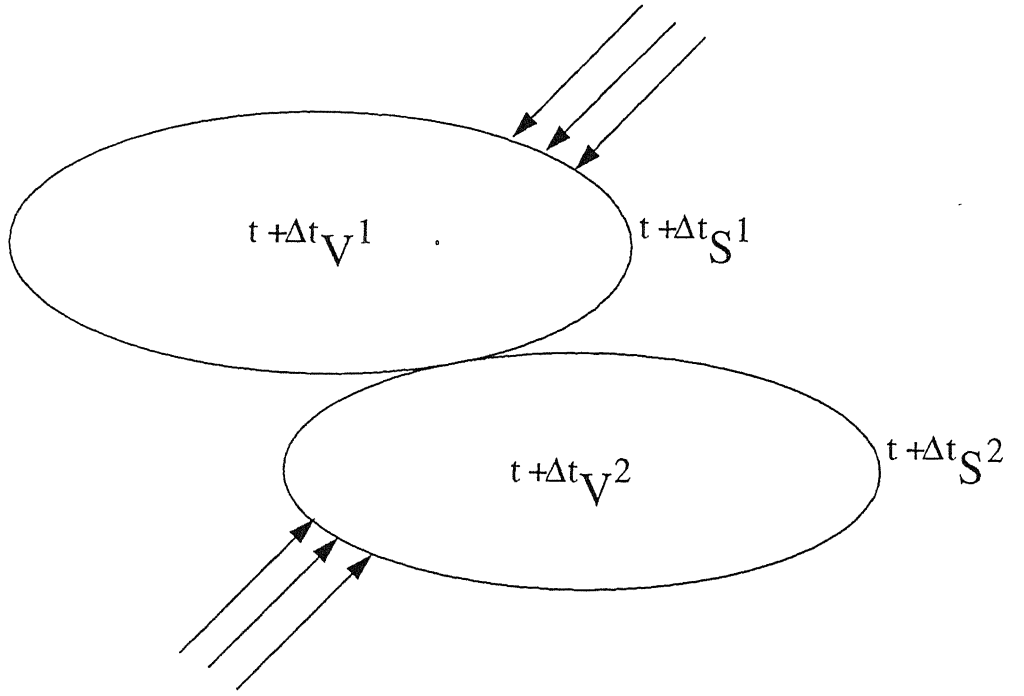


Figure 4.1: Two body contact system

smooth, outward unit normal vector at point¹ ${}^{t+\Delta t}\underline{x}^n$ on the boundary ${}^{t+\Delta t}S^n$ is denoted by ${}^{t+\Delta t}\underline{N}_1^n$. Other two orthonormal boundary vectors (in tangential directions) are ${}^{t+\Delta t}\underline{N}_2^n$ and ${}^{t+\Delta t}\underline{N}_3^n$ (see Figure (4.2)).

Suppose that two boundary points ${}^{t+\Delta t}\underline{x}^1$ and ${}^{t+\Delta t}\underline{x}^2$ are in contact with each other at time $t + \Delta t$ and the contact traction at ${}^{t+\Delta t}\underline{x}^n$ is denoted as ${}^{t+\Delta t}\underline{T}_c^n$. Then by Newton's third law of motion, we have:

$${}^{t+\Delta t}\underline{T}_c^1 = - {}^{t+\Delta t}\underline{T}_c^2 \quad (4.2)$$

where ${}^{t+\Delta t}\underline{T}_c^n$ can be expressed as:

$${}^{t+\Delta t}\underline{T}_c^n = \sum_{i=1}^3 {}^{t+\Delta t}t_i^n {}^{t+\Delta t}\underline{N}_i^n \quad (4.3)$$

where, ${}^{t+\Delta t}t_i^n$ denotes the component of ${}^{t+\Delta t}\underline{T}_c^n$ along ${}^{t+\Delta t}\underline{N}_i^n$.

If the two contact bodies are not welded together, then the normal component of traction can not be tensile. Thus we have:

$${}^{t+\Delta t}t_1^n \leq 0 \quad (4.4)$$

Further, from the Coulomb friction law we have:

$$\sqrt{({}^{t+\Delta t}t_2^n)^2 + ({}^{t+\Delta t}t_3^n)^2} \leq \mu |{}^{t+\Delta t}t_1^n| \quad (4.5)$$

¹Vectors are denoted by a letter with underbar

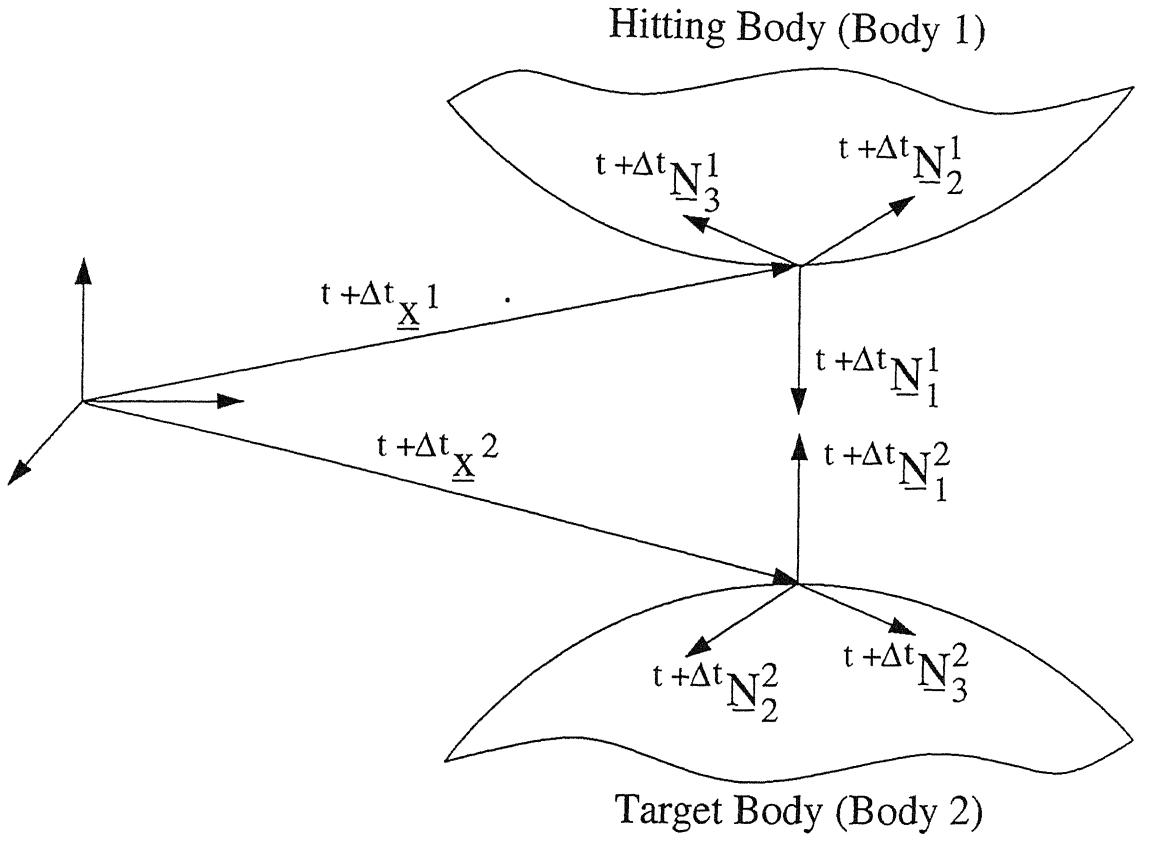


Figure 4.2: Points in contact and associated normal and tangent vectors

In equation (4.5), the “<” symbol represents the *sticking friction* and “=” represents the *slipping condition*. Further, the resultant tangential (friction) force is in the direction opposite to the relative velocity of slipping. The equations (4.4) and (4.5) represent *traction constraints*.

Physical considerations require that one body can not penetrate the other. Thus, for the points in contact, *penetration* must be zero. This condition can be mathematically stated as:

$${}^{t+\Delta t}p_1 = ({}^{t+\Delta t}\underline{x}^2 - {}^{t+\Delta t}\underline{x}^1) \cdot {}^{t+\Delta t}\underline{N}_1^2 = 0 \quad (4.6)$$

where ${}^{t+\Delta t}p_1$ represents the penetration between the two points in contact. In addition to (4.6), we need to have two more conditions to enforce the sticking friction, which ensure that there are no relative displacements (slip) between the contacting points in the tangential directions. These conditions can be stated as:

$${}^{t+\Delta t}p_2 = ({}^{t+\Delta t}\underline{x}^2 - {}^{t+\Delta t}\underline{x}^1) \cdot {}^{t+\Delta t}\underline{N}_2^2 = 0 \quad (4.7)$$

$${}^{t+\Delta t}p_3 = ({}^{t+\Delta t}\underline{x}^2 - {}^{t+\Delta t}\underline{x}^1) \cdot {}^{t+\Delta t}\underline{N}_3^2 = 0 \quad (4.8)$$

The conditions (4.6), (4.7) and (4.8) are called as the *kinematic constraints*.

4.2 Contact Force Expressions

As the contacting bodies are discretized for the purpose of developing finite element equations, the contact boundary gets automatically divided into surface elements, called as *contact segments*. The contact force formulation in this work employs a node-to-surface interface model, since this work deals with a large deformation problem including slipping at the contact interface. Normally in a contact formulation, contact is considered only at discrete nodes. Here, it is assumed that a node of the *hitting body* (body 1) comes into contact with a segment of the *target body* (body 2). The first step in the development of the contact force expression is the determination of the unit normal and tangent vectors at a point on the target segment. This is described in the next paragraph.

Geometry of a target segment can be described using 2-D shape functions. Thus,

$${}^{t+\Delta t}\underline{x}^2(\xi, \eta) = \sum_{j=1}^N \Phi_j(\xi, \eta) {}^{t+\Delta t}\underline{x}_j^2 \quad (4.9)$$

where, $\Phi_j(\xi, \eta)$ are the shape functions, ${}^{t+\Delta t}\underline{x}_j^2$ denotes the nodal position vector and N is the number of nodes per target segment. The side of a segment on which contact can occur is referred to as the positive side of the segment and the other side as the negative side of the segment. The local numbering of the nodes on a contact segment should be counter clockwise when we face the positive side of the segment. This is to get the correct sense for the outward normal vector at given point. A normal vector at point ${}^{t+\Delta t}\underline{x}^2(\xi, \eta)$ on the positive side of the segment is defined as:

$${}^{t+\Delta t}\underline{N}_1^2 = {}^{t+\Delta t}\underline{N}_\xi^2 \times {}^{t+\Delta t}\underline{N}_\eta^2 \quad (4.10)$$

where, ${}^{t+\Delta t}\underline{N}_\xi^2$ and ${}^{t+\Delta t}\underline{N}_\eta^2$ are the two tangent vectors at ${}^{t+\Delta t}\underline{x}^2(\xi, \eta)$ given by:

$${}^{t+\Delta t}\underline{N}_\xi^2 = {}^{t+\Delta t}\underline{x}^2(\xi, \eta)_{,\xi} \quad (4.11)$$

$${}^{t+\Delta t}\underline{N}_\eta^2 = {}^{t+\Delta t}\underline{x}^2(\xi, \eta)_{,\eta} \quad (4.12)$$

The unit normal and tangent vectors are defined as:

$${}^{t+\Delta t}\underline{N}_1^2 = {}^{t+\Delta t}\underline{N}_1^2 / |{}^{t+\Delta t}\underline{N}_1^2| \quad (4.13)$$

$${}^{t+\Delta t}\underline{N}_2^2 = {}^{t+\Delta t}\underline{N}_\xi^2 / |{}^{t+\Delta t}\underline{N}_\xi^2| \quad (4.14)$$

$${}^{t+\Delta t}\underline{N}_3^2 = {}^{t+\Delta t}\underline{N}_\eta^2 / |{}^{t+\Delta t}\underline{N}_\eta^2| \quad (4.15)$$

Since the contact is considered only at discrete hitting nodes, we can deal only with point forces at hitting nodes rather than with contact tractions. At time $t + \Delta t$, let

${}^{t+\Delta t}\{F^2\}$ be an array of Cartesian components of point force vector ${}^{t+\Delta t}\underline{F}^2$ at a point of the target segment at which the hitting node makes contact. By Newton's third law, the force vector on the hitting node will be $-{}^{t+\Delta t}\{F^2\}$.

Let ${}^{t+\Delta t}\{\delta u^2\}$ and ${}^{t+\Delta t}\{\delta u^1\}$ be the virtual displacement vectors at time $t + \Delta t$ at these points (on the target and hitting bodies respectively), when they come in contact. Then the virtual work at hitting node can be expressed as:²

$$\delta w_c = {}^{t+\Delta t}\{\delta u^2 - \delta u^1\}^T {}^{t+\Delta t}\{F^2\} \quad (4.16)$$

Note that the elements of ${}^{t+\Delta t}\{\delta u^1\}$, namely $\delta {}^{t+\Delta t}u^1$, $\delta {}^{t+\Delta t}v^1$, $\delta {}^{t+\Delta t}w^1$ are the virtual nodal displacements of the hitting node. The elements of ${}^{t+\Delta t}\{\delta u^2\}$ can be expressed in terms of the virtual nodal displacements of the target segment ($\delta {}^{t+\Delta t}u_i^2$, $\delta {}^{t+\Delta t}v_i^2$, $\delta {}^{t+\Delta t}w_i^2$, $i = 1, N$) using the 2-D shape functions (Φ_i , $i = 1, N$). Thus:

$${}^{t+\Delta t}\{\delta u^2 - \delta u^1\} = [Q_c] {}^{t+\Delta t}\{\delta u_c\} \quad (4.17)$$

where,

$$[Q_c] = \begin{bmatrix} -1 & 0 & 0 & \Phi_1 & 0 & 0 & \Phi_2 & 0 & 0 & . & . & . & \Phi_N & 0 & 0 \\ 0 & -1 & 0 & 0 & \Phi_1 & 0 & 0 & \Phi_2 & 0 & . & . & . & 0 & \Phi_N & 0 \\ 0 & 0 & -1 & 0 & 0 & \Phi_1 & 0 & 0 & \Phi_2 & . & . & . & 0 & 0 & \Phi_N \end{bmatrix} \quad (4.18)$$

and

$${}^{t+\Delta t}\{\delta u_c\}^T = \{\delta {}^{t+\Delta t}u^1, \delta {}^{t+\Delta t}v^1, \delta {}^{t+\Delta t}w^1, \delta {}^{t+\Delta t}u_1^2, \delta {}^{t+\Delta t}v_1^2, \delta {}^{t+\Delta t}w_1^2, \dots, \delta {}^{t+\Delta t}u_N^2\} \quad (4.19)$$

4.2.1 Sticking Friction Condition

For the sticking friction, the vector ${}^{t+\Delta t}\{F^2\}$ can be expressed as:

$${}^{t+\Delta t}\{F^2\} = \begin{bmatrix} {}^{t+\Delta t}N_{11}^2 & {}^{t+\Delta t}N_{21}^2 & {}^{t+\Delta t}N_{31}^2 \\ {}^{t+\Delta t}N_{12}^2 & {}^{t+\Delta t}N_{22}^2 & {}^{t+\Delta t}N_{32}^2 \\ {}^{t+\Delta t}N_{13}^2 & {}^{t+\Delta t}N_{23}^2 & {}^{t+\Delta t}N_{33}^2 \end{bmatrix} \begin{Bmatrix} {}^{t+\Delta t}f_1^2 \\ {}^{t+\Delta t}f_2^2 \\ {}^{t+\Delta t}f_3^2 \end{Bmatrix} \quad (4.20)$$

or,

$${}^{t+\Delta t}\{F^2\} = {}^{t+\Delta t}[N^2] {}^{t+\Delta t}\{f^2\} \quad (4.21)$$

where, ${}^{t+\Delta t}N_{ij}^2$ represents the j^{th} Cartesian component of the unit vector ${}^{t+\Delta t}\underline{N}_i^2$ and ${}^{t+\Delta t}f_i^2$ are the components, with respect to ${}^{t+\Delta t}\underline{N}_i^2$, of the contact force vector ${}^{t+\Delta t}\underline{F}^2$. Combining

²In this section, the right superscript denoting the iteration number has been omitted for convenience

the equations (4.16), (4.17) and (4.21), we get the following expression for the virtual work at the hitting node:

$$\delta w_c = {}^{t+\Delta t}\{\delta u_c\}^T {}^{t+\Delta t}\{r_c\} \quad (4.22)$$

where the vector ${}^{t+\Delta t}\{r_c\}$ is given by:

$${}^{t+\Delta t}\{r_c\} = [Q_c]^T {}^{t+\Delta t}[N^2] {}^{t+\Delta t}\{f^2\} \quad (4.23)$$

This is the contact force expression for a *sticking node* (hitting node, which is under sticking friction condition).

4.2.2 Slipping Condition

The contact force expression for a *slipping node* (hitting node, which is slipping on the target segment) is developed below:

The vector ${}^{t+\Delta t}\{r_c\}$ in equation (4.23) can be split as a contribution from the normal contact forces and tangential contact forces. Thus,

$${}^{t+\Delta t}\{r_c\} = {}^{t+\Delta t}\{r_n\} + {}^{t+\Delta t}\{r_t\} \quad (4.24)$$

where,

$${}^{t+\Delta t}\{r_n\} = [Q_c]^T {}^{t+\Delta t}\{N_1^2\} {}^{t+\Delta t}f_1^2 \quad (4.25)$$

and

$${}^{t+\Delta t}\{r_t\} = [Q_c]^T \left({}^{t+\Delta t}\{N_2^2\} {}^{t+\Delta t}f_2^2 + {}^{t+\Delta t}\{N_3^2\} {}^{t+\Delta t}f_3^2 \right) \quad (4.26)$$

Here, the arrays ${}^{t+\Delta t}\{N_i^2\}$, $i = 1, 2, 3$ contain the Cartesian components of the vector ${}^{t+\Delta t}\underline{N}_i^2$.

The three components of contact forces are not independent for a slipping node. From Coulomb's friction law, we have the relation:

$$\sqrt{({}^{t+\Delta t}f_2^2)^2 + ({}^{t+\Delta t}f_3^2)^2} = \mu |{}^{t+\Delta t}f_1^2| \quad (4.27)$$

where μ is the coefficient of friction, for a slipping node. Therefore, the tangential components of the contact forces can be written as:

$${}^{t+\Delta t}f_2^2 = -{}^{t+\Delta t}f_1^2 \mu \cos \theta \quad (4.28)$$

$${}^{t+\Delta t}f_3^2 = -{}^{t+\Delta t}f_1^2 \mu \sin \theta \quad (4.29)$$

where, θ is the angle between the resultant tangential (friction) force and the vector ${}^{t+\Delta t}\underline{N}_2^2$ and since the normal contact force is always compressive, “-” sign is used in the right hand side of both the above equations.

Calculation of the angle θ :

The friction force in the case of slipping is in a direction opposite to the relative velocity of slipping, which is same as the difference in incremental displacement of the target point and the hitting node. Therefore, the direction of the friction force on the target body is given by: $-\{ {}_t\Delta u^2 - {}_t\Delta u^1 \}_t = -([Q_c] {}_t\{\Delta u_c\})_t$, where the right subscript t indicates the tangential component. Define:

$${}_t\Delta \bar{u}_2 = - {}^{t+\Delta t}\{N_2^2\}^T [Q_c] {}_t\{\Delta u_c\} \quad (4.30)$$

$${}_t\Delta \bar{u}_3 = - {}^{t+\Delta t}\{N_3^2\}^T [Q_c] {}_t\{\Delta u_c\} \quad (4.31)$$

Thus, the angle θ is given by:

$$\theta = \tan^{-1} \left(\frac{{}_t\Delta \bar{u}_3}{{}_t\Delta \bar{u}_2} \right) \quad (4.32)$$

However, to avoid the difficulty in handling *infinity*, the computer implementation uses *cosine* function instead of *tangent* function for calculating θ .

Using equations (4.28) and (4.29) in equation (4.26) and substituting equations (4.25) and (4.26) in equation (4.24) we get:

$${}^{t+\Delta t}\{r_c\} = [Q_c]^T \left({}^{t+\Delta t}\{N_1^2\} - {}^{t+\Delta t}\{N_2^2\} \mu \cos \theta - {}^{t+\Delta t}\{N_3^2\} \mu \sin \theta \right) {}^{t+\Delta t}f_1^2 \quad (4.33)$$

4.3 Kinematic Constraints in Nodal Form

The kinematic constraints should be written separately for the sticking nodes and for slipping nodes.

4.3.1 Sticking Friction Condition

To express the kinematic constraints in terms of the nodal displacements, the equations (4.6), (4.7) and (4.8) are combined in matrix form for the i^{th} Newton-Raphson iteration as:

$${}^{t+\Delta t}\{p\}^{(i)} = {}^{t+\Delta t}[N^2]^T {}^{t+\Delta t}\{x^2 - x^1\}^{(i)} \quad (4.34)$$

where,

$${}^{t+\Delta t}\{p\}^{(i)T} = \{{}^{t+\Delta t}p_1^{(i)}, {}^{t+\Delta t}p_2^{(i)}, {}^{t+\Delta t}p_3^{(i)}\} \quad (4.35)$$

We have,

$${}^{t+\Delta t}\{x^2 - x^1\}^{(i)} = {}^{t+\Delta t}\{x^2 - x^1\}^{(i-1)} + {}_t\{\Delta u^2 - \Delta u^1\}^{(i)} \quad (4.36)$$

where, the second term on the right hand side is an array of Cartesian components of the difference of the displacement vectors of the target and hitting bodies at the contact node, for the current iteration. For the first iteration:

$${}^{t+\Delta t}\{x^2 - x^1\}^{(i-1)} = {}^{t+\Delta t}\{x^2 - x^1\}^{(0)} = {}_t\{x^2 - x^1\} \quad (4.37)$$

Analogous to equation (4.17), this can be written as:

$${}_t\{\Delta u^2 - \Delta u^1\}^{(i)} = [Q_c] {}_t\{\Delta u_c\}^{(i)} \quad (4.38)$$

where, the vector ${}_t\{\Delta u_c\}^{(i)}$ given by:

$${}_t\{\Delta u_c\}^{(i)T} = \{{}_t\Delta u^1^{(i)}, {}_t\Delta v^1^{(i)}, {}_t\Delta w^1^{(i)}, {}_t\Delta u_1^2^{(i)}, {}_t\Delta v_1^2^{(i)}, {}_t\Delta w_1^2^{(i)}, \dots, {}_t\Delta w_N^2^{(i)}\} \quad (4.39)$$

contains the nodal values of displacement at the hitting node and the nodes of the target segment for the current iteration. Recognizing the first term of the right hand side of the equation (4.36) as corresponding to ${}^{t+\Delta t}\{p\}^{(i-1)}$ (penetration for the previous iteration), equation (4.36) can be written as:

$${}^{t+\Delta t}\{p\}^{(i)} = {}^{t+\Delta t}\{p\}^{(i-1)} + {}^{t+\Delta t}[N^2]^T [Q_c] {}_t\{\Delta u_c\}^{(i)} \quad (4.40)$$

For the first iteration,

$${}^{t+\Delta t}\{p\}^{(i-1)} = {}^{t+\Delta t}\{p\}^{(0)} = {}_t\{p\} \quad (4.41)$$

Therefore, the kinematic constraints for sticking node is:

$${}^{t+\Delta t}\{p\}^{(i-1)} + {}^{t+\Delta t}[N^2]^T [Q_c] {}_t\{\Delta u_c\}^{(i)} = \{0\} \quad (4.42)$$

The first term of the right hand side of equation (4.36), on similar development gives:

$${}^{t+\Delta t}\{p\}^{(i-1)} = {}^{t+\Delta t}[N^2]^T [Q_c] {}^{t+\Delta t}\{x_c\}^{(i-1)} \quad (4.43)$$

where, ${}^{t+\Delta t}\{x_c\}^{(i-1)}$ is the array of coordinates of the hitting node and of the nodes of the target segment updated upto the previous iteration.

4.3.2 Slipping Condition

The development of the nodal constraints for the slipping nodes is similar to the sticking friction condition, except that we have only one kinematic constraint, viz., the equation (4.6).

We can write the matrix form of the kinematic constraints for the i^{th} Newton-Raphson iteration as:

$${}^{t+\Delta t}p_1^{(i)} = {}^{t+\Delta t}\{N_1^2\}^T {}^{t+\Delta t}\{x^2 - x^1\}^{(i)} \quad (4.44)$$

Using the equations (4.35 – 4.39) in (4.44) we get:

$${}^{t+\Delta t}p_1^{(i)} = {}^{t+\Delta t}p_1^{(i-1)} + {}^{t+\Delta t}\{N_1^2\}^T [Q_c] {}^t\{\Delta u_c\}^{(i)} \quad (4.45)$$

For the first iteration,

$${}^{t+\Delta t}p_1^{(i-1)} = {}^{t+\Delta t}p_1^{(0)} = {}^tp_1 \quad (4.46)$$

Therefore, the kinematic constraint for a slipping node is:

$${}^{t+\Delta t}p_1^{(i-1)} + {}^{t+\Delta t}\{N_1^2\}^T [Q_c] {}^t\{\Delta u_c\}^{(i)} = 0 \quad (4.47)$$

Similar to the sticking condition, we have:

$${}^{t+\Delta t}p_1^{(i-1)} = {}^{t+\Delta t}\{N_1^2\}^T [Q_c] {}^{t+\Delta t}\{x_c\}^{(i-1)} \quad (4.48)$$

where, ${}^{t+\Delta t}\{x_c\}^{(i-1)}$ contains the coordinates of the hitting node and the nodes of target segment updated upto the previous iteration.

4.4 Lagrange Multiplier Method

In Lagrange Multiplier Method, the contact forces are considered as primary unknowns and the kinematic constraints are enforced exactly. We have the contact force expression for a sticking node given by equation (4.23) and for slipping node by equation (4.33). The kinematic constraint for sticking node is given by equation (4.42):

$${}^{t+\Delta t}[N^2]^T [Q_c] {}^t\{\Delta u_c\}^{(i)} = -{}^{t+\Delta t}\{p\}^{(i-1)} \quad (4.49)$$

and for a slipping node is given by equation (4.47):

$${}^{t+\Delta t}\{N_1^2\}^T [Q_c] {}^t\{\Delta u_c\}^{(i)} = -{}^{t+\Delta t}p_1^{(i-1)} \quad (4.50)$$

Combining the equations (4.23) and (4.49) we get for a sticking node,

$$\begin{bmatrix} 0 & -{}^{t+\Delta t}[q_1] \\ -{}^{t+\Delta t}[q_1]^T & 0 \end{bmatrix} \begin{Bmatrix} {}^{t+\Delta t}\{f^2\}^{(i)} \\ {}^t\{\Delta u_c\}^{(i)} \end{Bmatrix} = \begin{Bmatrix} {}^{t+\Delta t}\{p\}^{(i-1)} \\ -{}^{t+\Delta t}\{r_c\}^{(i)} \end{Bmatrix} \quad (4.51)$$

where,

$${}^{t+\Delta t}[q_1] = {}^{t+\Delta t}[N^2]^T [Q_c] \quad (4.52)$$

Combining the equations (4.33) and (4.50) we get for a slipping node,

$$\begin{bmatrix} 0 & -{}^{t+\Delta t}\{q_2\}^T \\ -{}^{t+\Delta t}\{q_3\} & 0 \end{bmatrix} \begin{Bmatrix} {}^{t+\Delta t}f_1^{(i)} \\ {}^t\{\Delta u_c\}^{(i)} \end{Bmatrix} = \begin{Bmatrix} {}^{t+\Delta t}p_1^{(i-1)} \\ -{}^{t+\Delta t}\{r_c\}^{(i)} \end{Bmatrix} \quad (4.53)$$

where,

$${}^{t+\Delta t}\{q_2\}^T = {}^{t+\Delta t}\{N_1^2\}^T [Q_c] \quad (4.54)$$

$${}^{t+\Delta t}\{q_3\} = [Q_c]^T \left({}^{t+\Delta t}\{N_1^2\} - {}^{t+\Delta t}\{N_2^2\} \mu \cos \theta - {}^{t+\Delta t}\{N_3^2\} \mu \sin \theta \right) \quad (4.55)$$

Assembling these equations over all the potential contact nodes, we get the following global equation:

$$\begin{bmatrix} 0 & -{}^{t+\Delta t}[Q_1] \\ -{}^{t+\Delta t}[Q_2]^T & 0 \end{bmatrix} \begin{Bmatrix} {}^{t+\Delta t}\{F^2\}^{(i)} \\ {}^t\{\Delta U_c\}^{(i)} \end{Bmatrix} = \begin{Bmatrix} {}^{t+\Delta t}\{P\}^{(i-1)} \\ -{}^{t+\Delta t}\{R_c\}^{(i)} \end{Bmatrix} \quad (4.56)$$

Note that, while the whole global coefficient matrix is known from the geometry, only a part of the right side vector, namely ${}^{t+\Delta t}\{P\}^{(i-1)}$ is known from the geometry. The other part, ${}^{t+\Delta t}\{R_c\}^{(i)}$, is unknown. This vector is eliminated by combining this equation with equation (3.58) of chapter 3. Before this, the set of equation (3.58) is condensed to retain only those degrees of freedoms, which are associated with the contact nodes. This condensed and combined set is solved to find the nodal displacements of the contact nodes and the contact forces. Then the equation (3.49) is used to find the displacements of nodes of type 2.

4.5 Algorithm used for Dynamic Large Deformation Elasto-plastic Contact Problem

For solving a typical dynamic, large deformation, elasto-plastic, contact problem, the following steps are used:

1. Finding the potential contact nodes for which the hitting and target nodes are closer than a prescribed length.
2. Renumbering the nodes: Nodes of the hitting and target nodes are renumbered such that the contact nodes are numbered first. This is carried out to facilitate the static condensation of the stiffness matrix which helps in reducing the computational time.
3. Coefficient matrix: Based on the current geometry and state of stress, condensed form of effective stiffness matrix and force vector is formed.
4. Begin the Newton-Raphson iteration.
5. Contact search: Search for the target segment corresponding to each hitting node. Master-slave algorithm is used here.
6. Contact iterations:
 - Initially all the potential nodes are assumed to be in sticking friction. Form the contact stiffness matrix and right side vector. Combine with the condensed form of the effective stiffness matrix and the effective force vector. Solve the system of equations.
 - Find the “out of contact” nodes, for which the normal component of the contact reaction is tensile (refer equation (4.4)). The contact reactions at these nodes are forced to be zero during the subsequent contact iterations.
 - After removing all the “out of contact” nodes, the nodes which are slipping are determined. We know that a node is slipping, if the contact reactions at that node violate equation (4.5), expressed in a nodal form.
 - Repeat the contact iterations till the correct direction of friction force is obtained for all the slipping nodes and no node changes the contact status.
7. Find the displacements of the non-contact nodes (type 2 nodes) from the displacements of type 1 nodes.
8. Updating: Update the stresses, strains and contact forces.
9. Convergence: Find out the unbalance force and check for convergence. If the Newton-Raphson iterations have converged, store the results at the end of the increment.

ment and start the next time increment. If the convergence criterion is not satisfied, repeat the Newton-Raphson iteration and continue till convergence.

Chapter 5

Results and Discussion

A finite element code for the analysis of 3-D, dynamic, elasto-plastic contact problem including the effect of friction is developed based on the formulations presented in the chapters 2, 3 and 4. The stiffness matrix, mass matrix and force vectors are evaluated using numerical integration, while Newmark's scheme is used to update the velocity and acceleration after each time-step. The code is developed for 8-noded brick element and 2-point Gauss-Legendre numerical integration is used in each direction. This chapter discusses the validation of the code and a study of an additional problem to show the application of the code to impact problems.

5.1 Validation

The validation of the code is necessary to prove the applicability of the program to the class of the problems of interest. Here, the validation is done by comparing the results obtained with the results reported in the published literature.

The code developed for dynamic large deformation elasto-plastic contact analysis is validated by using the following problems:

1. Elasto-plastic dynamic response of a simply supported square plate.
2. Oblique impact of two infinite blocks.
3. Impact of two cantilever beams.

5.1.1 Elasto-plastic Dynamic Response of a Simply Supported Square Plate

This is a single body analysis of an elasto-plastic, simply supported square plate subjected to a lateral step load of 300 psi, reported by Gendy and Saleeb [49]. The material is assumed to be *elastic-perfectly plastic*. The geometric and material properties of the plate as given in the reference [49] are given below:

- Length of side = 10 inches
- Thickness = 0.5 inches
- Young's modulus = 1×10^7 psi
- Poisson's ratio = 0.3
- Yield stress = 3×10^4 psi
- Density = 2.588×10^{-4} lb-sec²/in⁴

Due to the symmetry, only one quarter of the plate was modelled. The finite element model consist of 10 elements along the side (half length of the plate) and 4 elements along the thickness. The timestep used is 22.3×10^{-6} seconds, which is approximately equal to $(1/48)^{th}$ of the fundamental period of the linear elastic plate.

Since, the material model used in this work is based on a power law type hardening, it can not be used for an elastic-perfectly plastic material. However, the response for the elastic-perfectly plastic material can be obtained as the limiting case when $K \rightarrow 0$. Hence for different cases are considered, where K is reduced progressively: elastic material, elasto-plastic material with $K = 1 \times 10^6$ psi, $n = 1$, elasto-plastic material with $K = < 10^5$ psi, $n = 1$ and elasto-plastic material with $K = 1 \times 10^4$ psi, $n = 1$. For K smaller than 1×10^4 psi, not much change is observed in the response. Hence, this last case can be considered as the limiting case. The displacement at the center of the plate given in reference [49] and those obtained using the present code are shown in figures (5.1) and respectively. An excellent agreement in trends of the predicted time responses is observed. However, the displacements obtained in this work are slightly lesser than those given in [49]. This is mainly due to two reasons:

1. numerical inaccuracies associated with approximating an elastic-perfectly plastic material using a hardening type material model and
2. different types of finite elements used (Gendy and Saleeb [49] used higher order shell elements, while linear 8-noded brick element is used in this work).

Figures (5.3) and (5.4) give the variation of maximum equivalent stress and maximum equivalent plastic strain with time. It is observed that the stress increases slightly even after reaching the yield point, which is not the case for an elastic-perfectly plastic material.

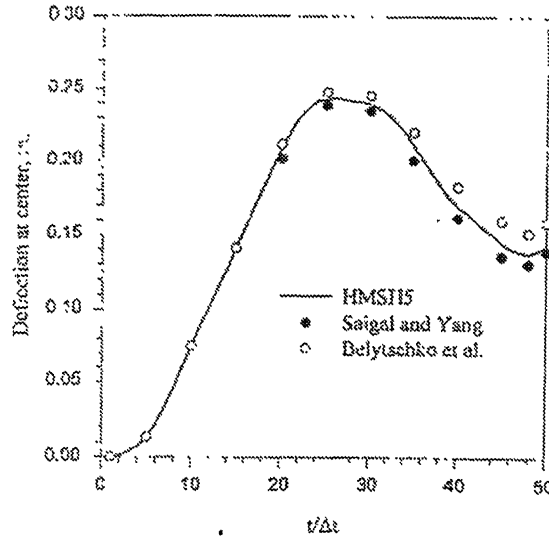


Figure 5.1: Displacement at the center of the plate (Ref. [49])

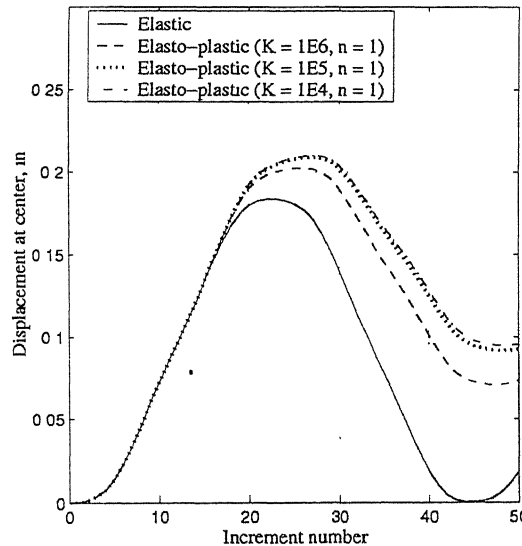


Figure 5.2: Displacement at the center of the plate (Present work)

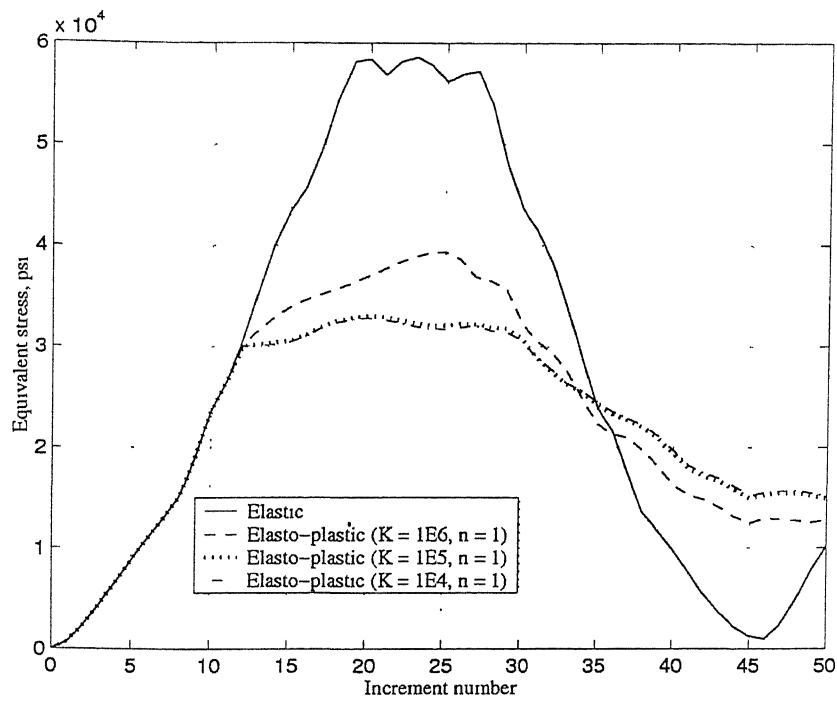


Figure 5.3: Maximum equivalent stress in the plate (Present work)

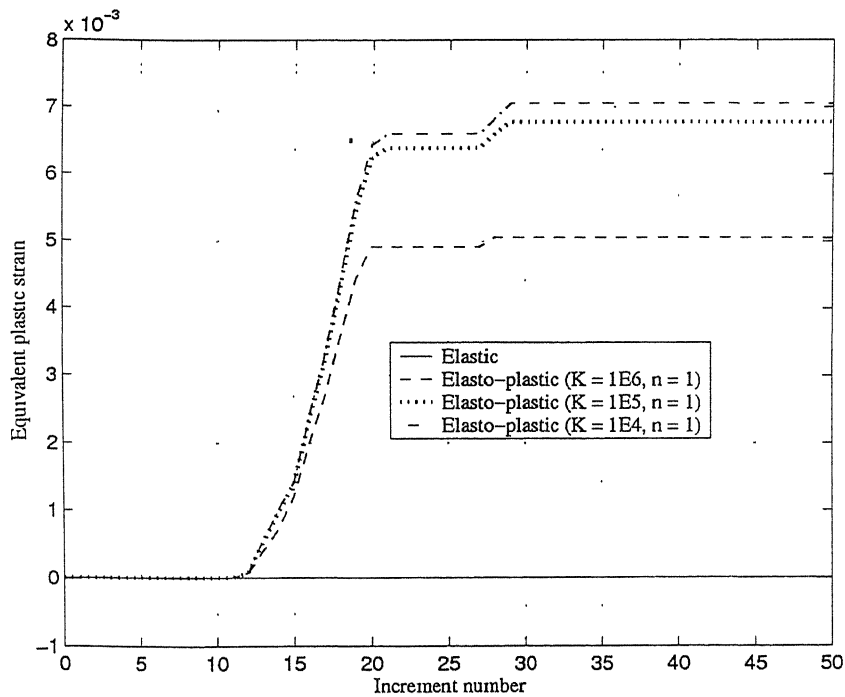


Figure 5.4: Maximum equivalent plastic strain in the plate (Present work)

5.1.2 Oblique Impact of Two Infinite Blocks

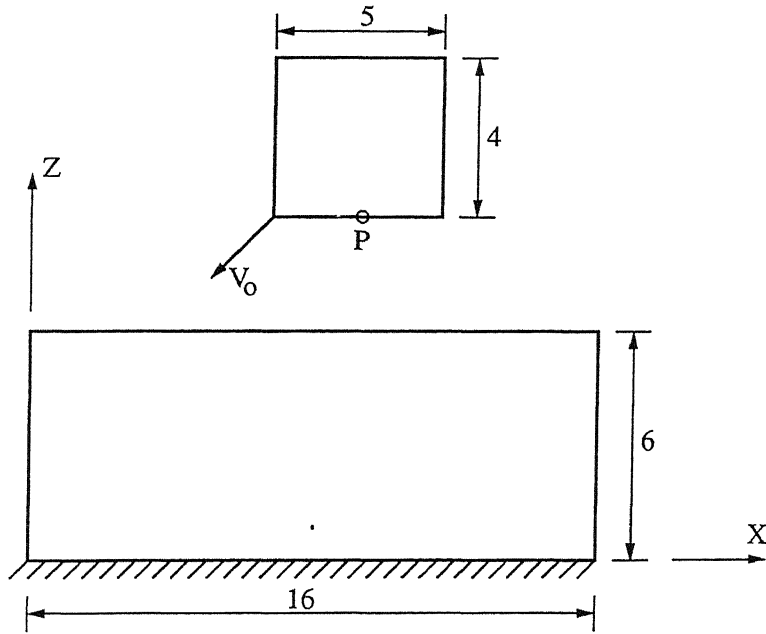


Figure 5.5: Oblique impact of two elastic blocks

The second problem used for validation is the oblique impact of two infinite elastic blocks (plane strain problem) shown in figure 5.5. This problem is reported in reference [43]. The top block is given a uniform initial velocity, $v_0 = (-10, 0, -10)$ units (in the coordinate system shown in figure). The geometric and material properties are:

- Hitting Block
 - length = 5 units
 - height = 4 units
- Target Block
 - length = 16 units
 - height = 6 units
- Young's Modulus (E) = 1000 units, for both the blocks.
- Poisson's ratio (ν) = 0.0, for both the blocks.
- Density (ρ) = 0.1 units, for both the blocks.

Armero and Petocz [43] have solved this problem as a plane strain problem. Bhat [50] has solved the same problem, only for the frictionless case, using Jaumann stress measure and Green-Lagrange strain measure. Since the Poisson's ratio is zero, the plane strain and plane stress formulations will give the same results. In this work, the problem is solved with only one element in the Y -direction. To overcome the numerical difficulty arising due to low stiffness in Y -direction, the displacement along this direction is fixed at all nodes for both the bodies.

The following are the discretization and timestep considered:

- Discretization:
 - Number of elements in the hitting block = $20 (5 \times 1 \times 4)$
 - Number of elements in the target block = $96 (16 \times 1 \times 6)$
 - Number of d.o.f in the hitting block = 180
 - Number of d.o.f in the target block = 714
- Time-step = 0.01 units

There are two different cases. In the first case, there is no friction at contact interface and in the second case friction coefficient (μ) between the hitting and target bodies is 0.4.

The X and Z displacements at point P are plotted against the time. The Y direction used in reference [43] is the Z -direction in this work. Both the displacements and time are measured from the instant of contact between the two blocks. The results reported in [43] are given in figures (5.6) and (5.8) and those obtained from the present code are shown in figures (5.7) & (5.9). The results are found to be in good agreement.

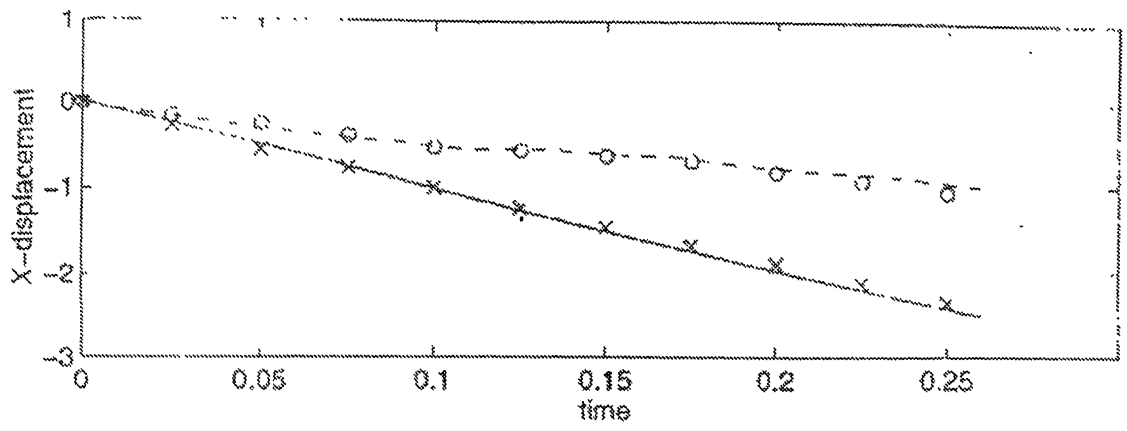


Figure 5.6: X-displacement of point P (Ref. [43])

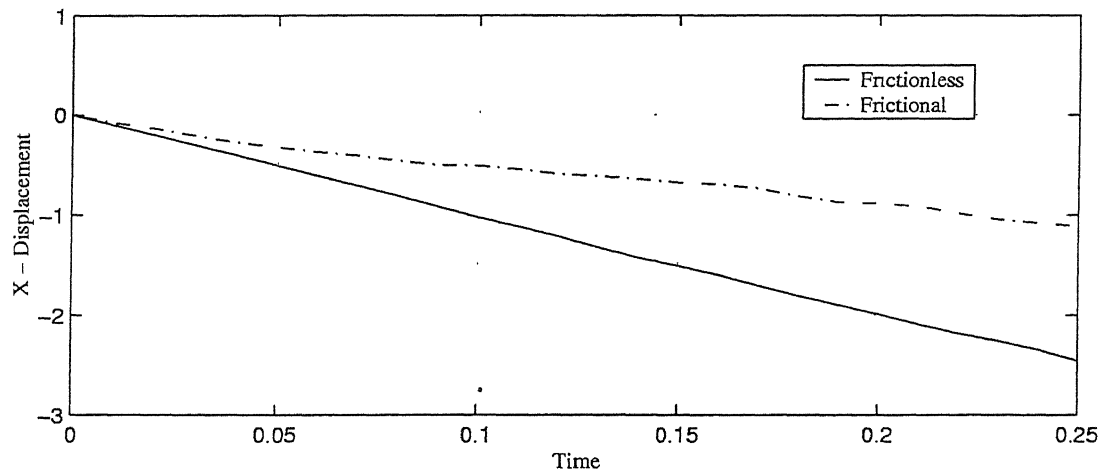


Figure 5.7: X-displacement of point P (present work)

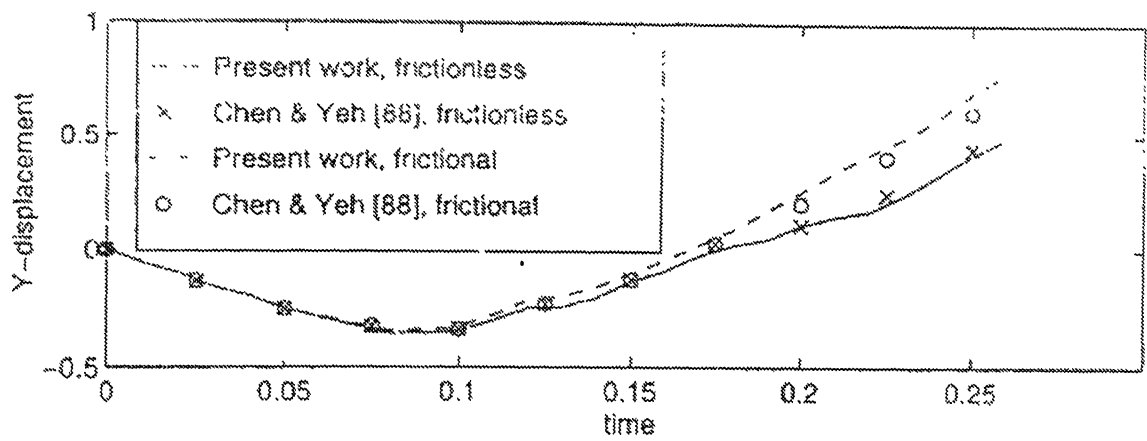


Figure 5.8: Y-displacement of point P (Ref. [43])

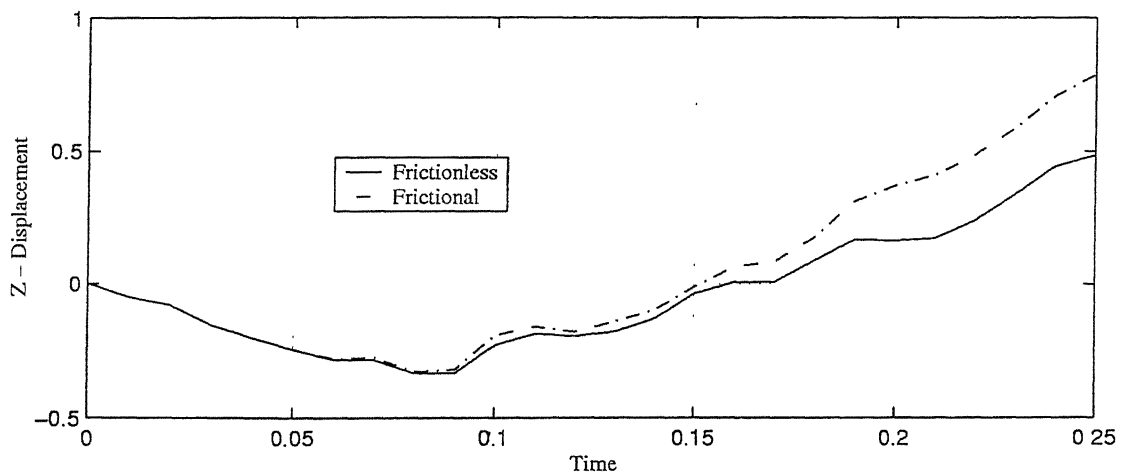


Figure 5.9: Z-displacement of point P (Present work)

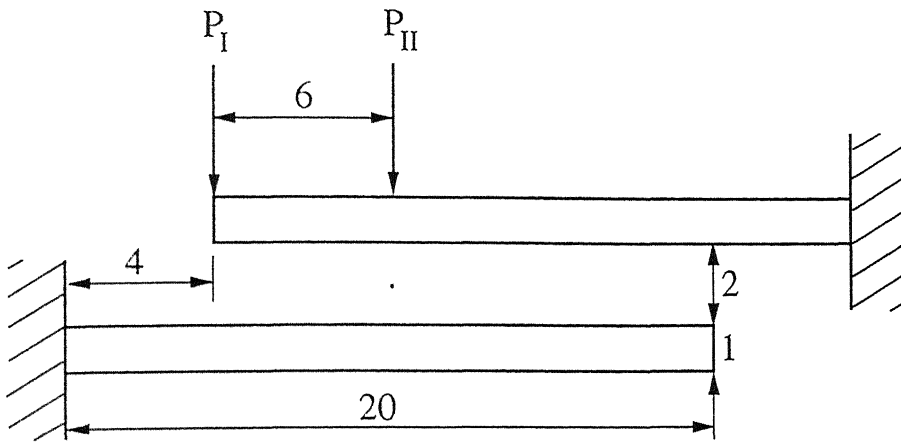


Figure 5.10: Impact of two cantilever beams

5.1.3 Impact of two Cantilever Beams

This is a large deformation, elastic, plane stress problem given in reference [35]. Both the cantilever beams are identical and fixed at different ends as shown in figure (5.10). The geometric and material properties are given below:

- Length of cantilever = 20 units
- Height of cantilever = 1 unit
- Thickness of cantilever = 0.01 units
- Density = 4 units
- Young's modulus = 4000 units
- Poisson's ratio = 0.3

There are two cases of external loading P_I and P_{II} each with a magnitude 0.15 units and three cases of friction ($\mu = 0.0, 0.2, 0.4$) for each case of loading.

Sung and Kwak [35] have done the problem using plane stress formulation. To do this problem using three dimensional problem, we have to prevent the twisting of the cantilever, produced due to the errors associated with numerical computation. This objective is achieved by modelling only half of the cantilevers and applying the symmetry boundary conditions at the mid-plane.

The discretization and time-step size are given below:

- Number of elements for each cantilever = 80 ($40 \times 1 \times 2$)

- Number of dof for each cantilever = 738
- Time-step size = 0.015 units

The Horizontal and vertical displacements of the end tip of the upper cantilver reported in Sung and Kwak [35] are given in figures (5.11) and (5.13) and those from obtained in this work are given in figures (5.12) and (5.14). It is found that, for the frictionless case, the horizontal displacements are closely matching till time = 10 units. Beyond this time, the results from this work are substantially higher than those reported by Sung and Kwak [35]. The agreement is better for the vertical displacements, which show close matching with the reported results till time = 14 units for case PII and till divergence (time = 11.25) for case PI. The difference in the results in the later time incerements may be due to the numerical errors accumulated over the increments and due to the differences created by plane stress and 3-D formulations.

For the cases where there is friction, convergence difficulties are observed, even after using the divergence handling algorithms. The analysis could be completed only for the loadcase PI, with coefficient of friction $\mu = 0.2$. The results obtained for this case also are shown in figures (5.12) and (5.14). The results show good agreement for horizontal displacement till time = 8 units and for vertical displacements till time = 14 units, with those reported by Sung and Kwak [35].

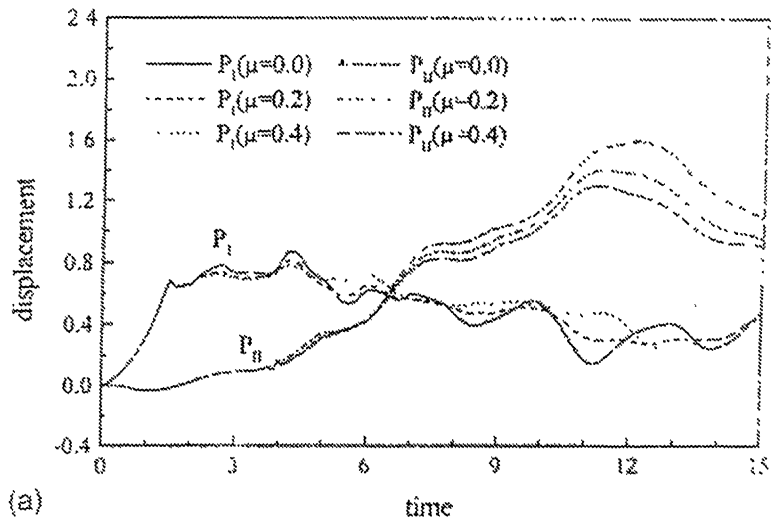


Figure 5.11: Horizontal displacement at the end tip of upper cantilever (Ref. [35])

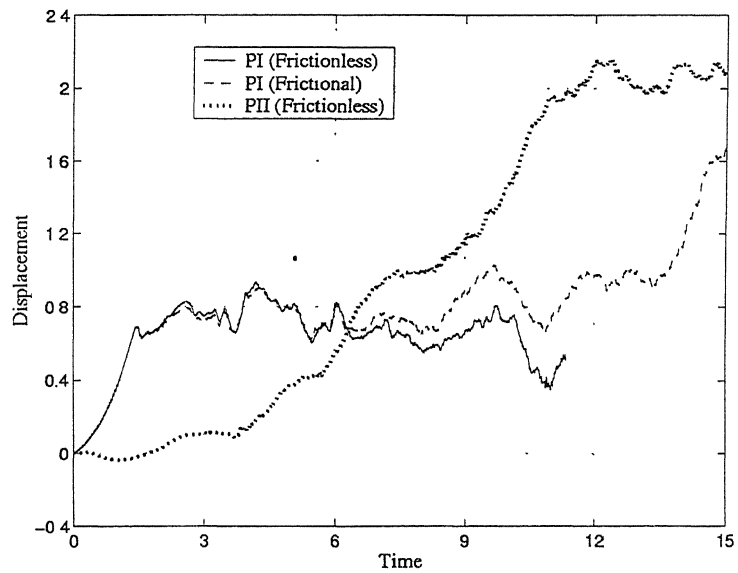


Figure 5.12: Horizontal displacement at the end tip of upper cantilever (Present work)

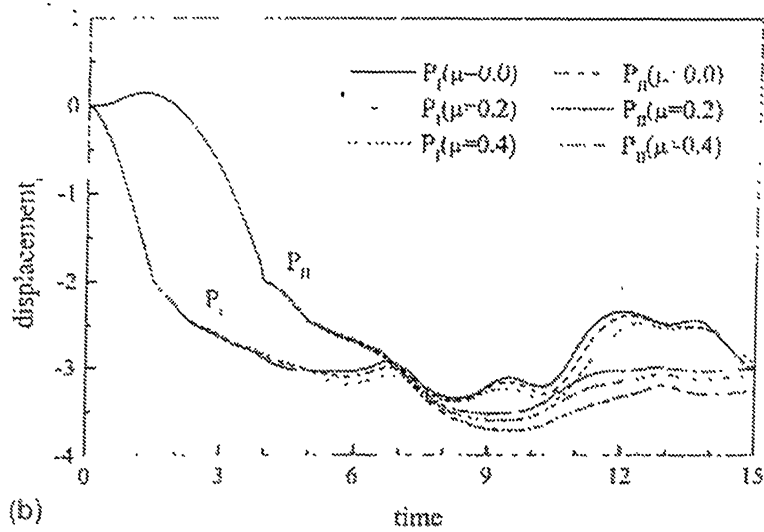


Figure 5.13: Vertical displacement at the end tip of upper cantilever (Ref. [35])

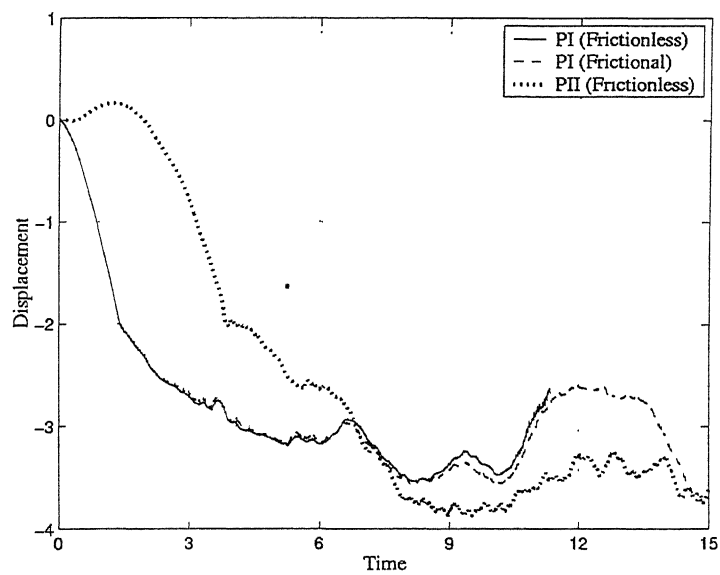


Figure 5.14: Vertical displacement at the end tip of upper cantilever (Present work)

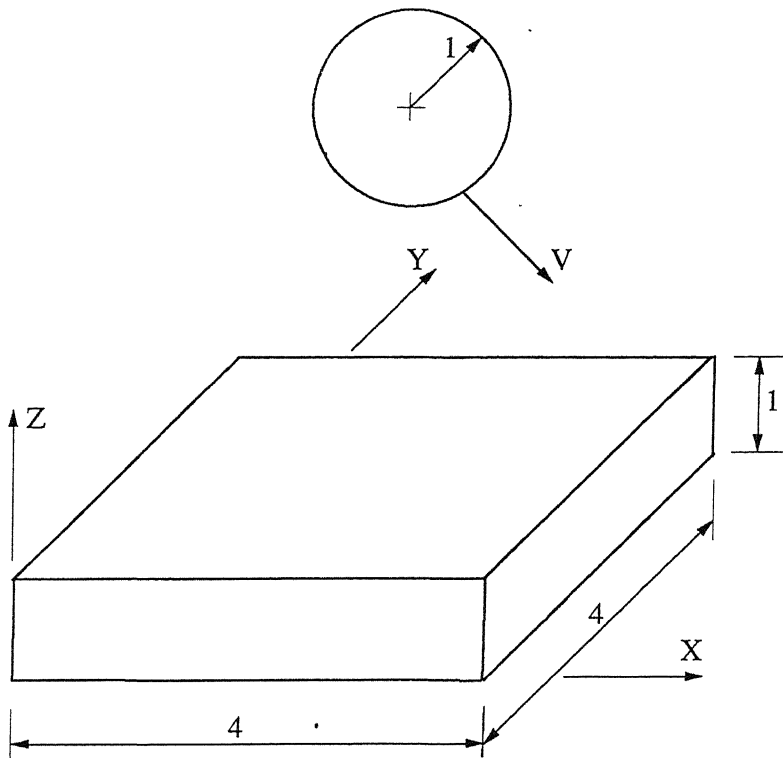


Figure 5.15: Impact of a sphere on plate

5.1.4 Elasto-plastic Impact of a Sphere on a Plate with Friction

To demonstrate the applicability of the program developed, elasto-plastic impact of a sphere on a plate is analyzed (See figure (5.15)). Two different cases, viz., frictionless contact and contact with friction interphase ($\mu = 0.2$) are considered. The sphere is given an initial velocity, $V = (10, 0, -10)$, in the coordinate system shown.

The geometric details of the sphere and plate are shown in figure (5.15). The material properties assumed for both the bodies are as follows:

- Young's modulus (E) = 4×10^5 units
- Poisson's ratio (ν) = 0.3
- Density (ρ) = 4 units
- Yield Strength ($(\sigma_y)_0$) = 5000 units
- Hardening coefficient (K) = 40000 units
- Hardening exponent (n) = 0.4

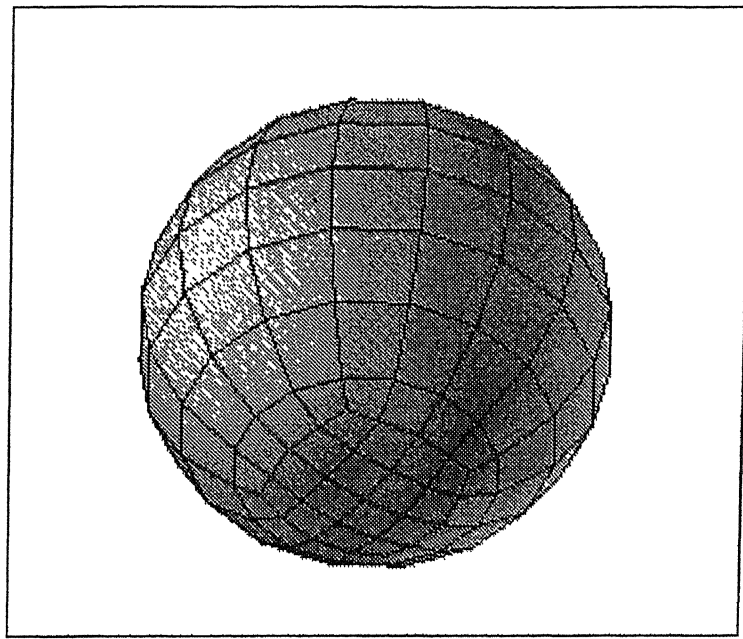


Figure 5.16: Finite element plot of sphere (Full view)

The plate is fixed along the edges. Time step used for the analysis is 0.002 units. The mesh details of the plate and sphere are as follows:

- Number of elements for sphere = 672 (Refer figures (5.16) and (5.17))
- Number of elements for plate = 1024 ($16 \times 16 \times 4$)
- Number of d.o.f. for sphere = 2319
- Number of d.o.f. for plate = 4335

The plots of the configurations of sphere and plate at different times are given in figures (5.18 – 5.21) for frictionless case and in figures (5.22 – 5.25) for the frictional case. The X and Z displacements of the bottom node and the centre of the sphere for both the frictionless and the frictional cases are shown in figures (5.26) and (5.27). It is observed that the displacement along the X -direction is significantly lesser for the frictional case, more so at the bottom node. Further, in the frictional case, the X -displacement plots of centre and bottom nodes are very much different, while they are almost same in the frictionless case. This is due to the rotation of the sphere induced by the frictional forces, which reduce the displacement along X -direction, but increase the displacement along Z -direction at the bottom node. This rotation of the sphere in the frictional case is clearly seen in figures (5.22 – 5.25). Also, it is observed that the displacement along negative

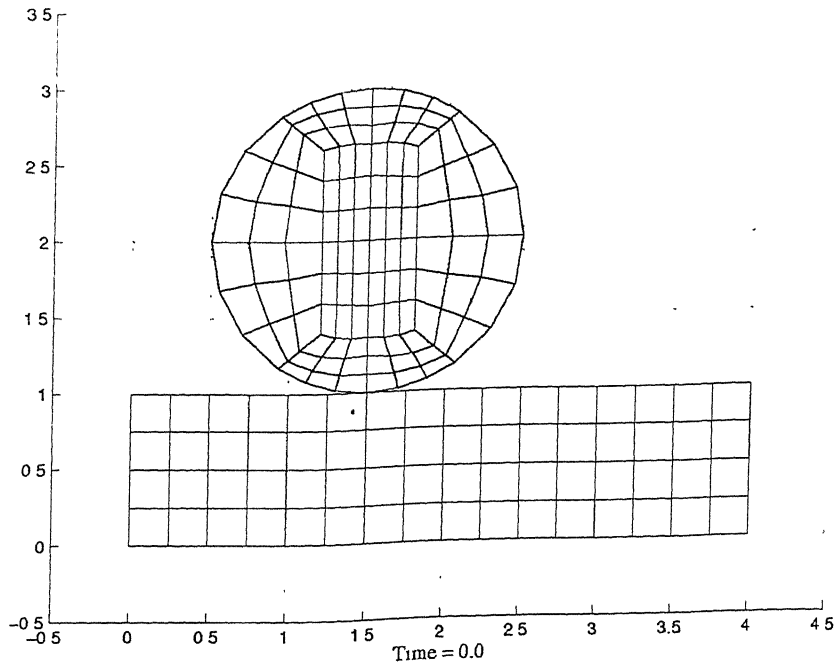


Figure 5.18: Impact of sphere on plate (Frictionless): Configuration at $t = 0.0$

The velocity given to the sphere is $(10,0,-10)$ m/s, in the coordinate system shown in figure (5.15) and the coefficient of friction at the contact interface is 0.3, for the case of analysis with friction. The time step used in this analysis is 0.0003 seconds. The X and Z displacements of the bottom node and the centre of the sphere for both the frictionless and the frictional cases are shown in figures (5.29) and (5.30). The variation of maximum equivalent stress in both the sphere and plate for both cases is shown in figure (5.31). Convergence difficulties are observed in the frictional case, and the analysis could be done till 0.0123 seconds, while the contact between the bodies are lost at about 0.02 seconds.

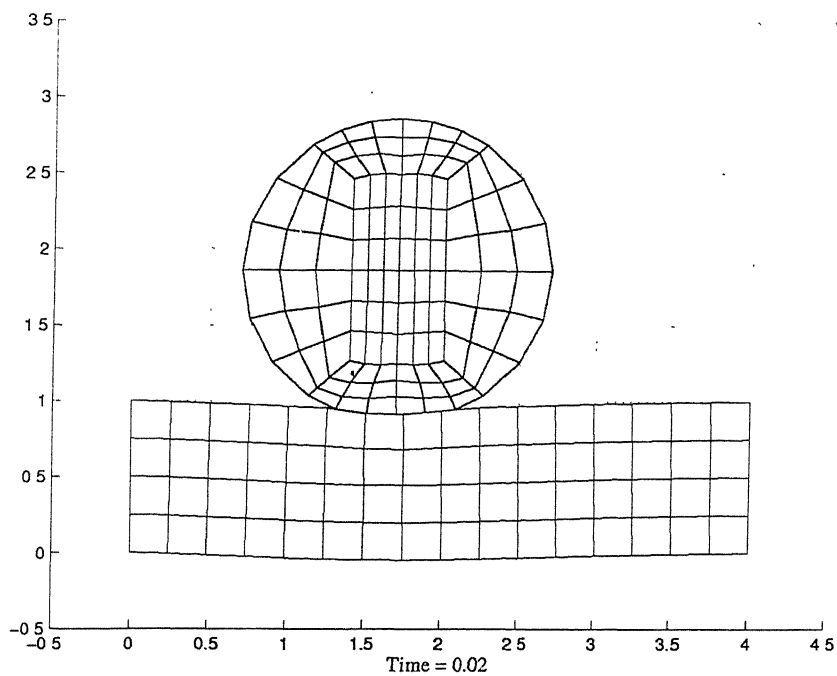


Figure 5.19: Impact of sphere on plate (Frictionless): Configuration at $t = 0.02$

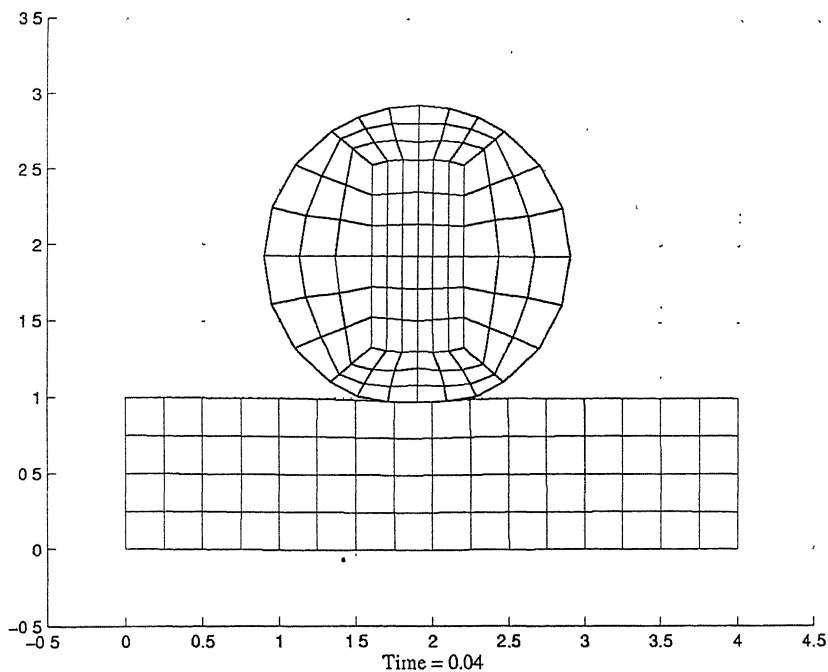


Figure 5.20: Impact of sphere on plate (Frictionless): Configuration at $t = 0.04$

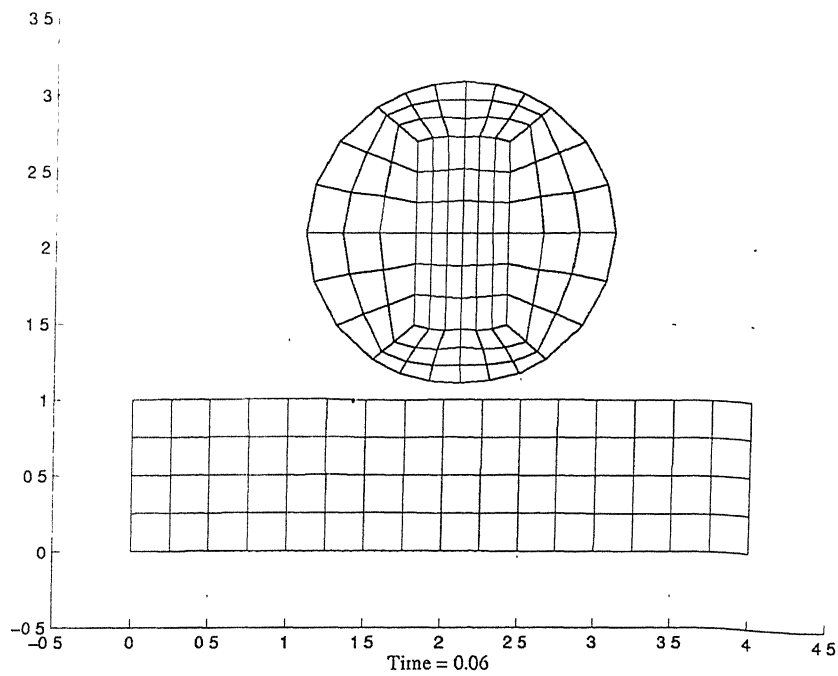


Figure 5.21: Impact of sphere on plate (Frictionless): Configuration at $t = 0.06$

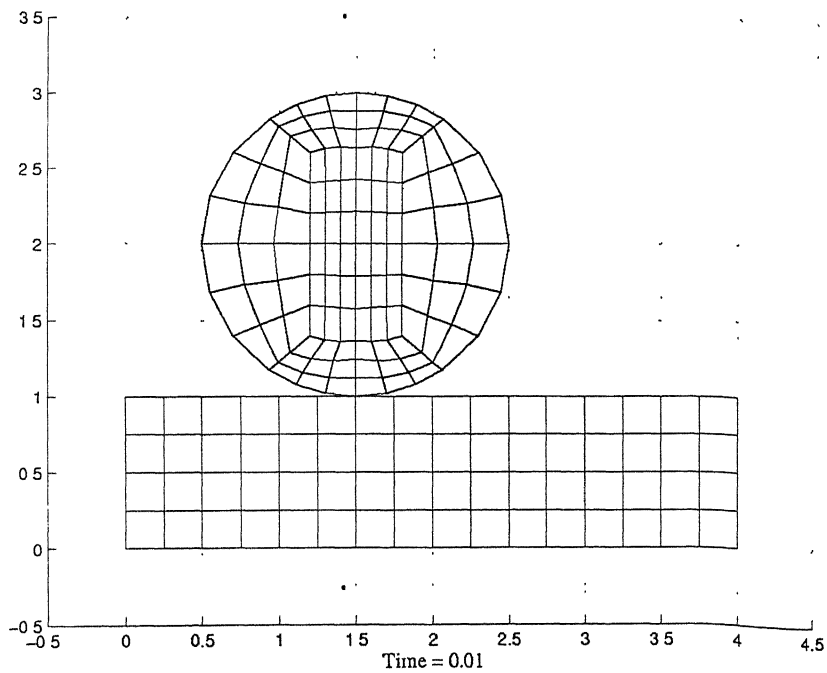


Figure 5.22: Impact of sphere on plate (Frictional): Configuration at $t = 0.0$

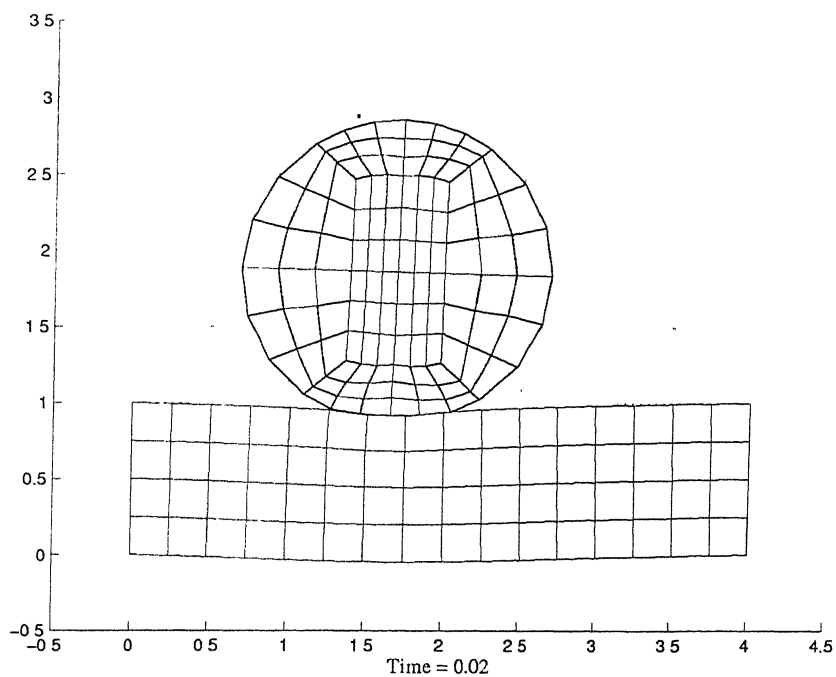


Figure 5.23: Impact of sphere on plate (Frictional): Configuration at $t = 0.02$

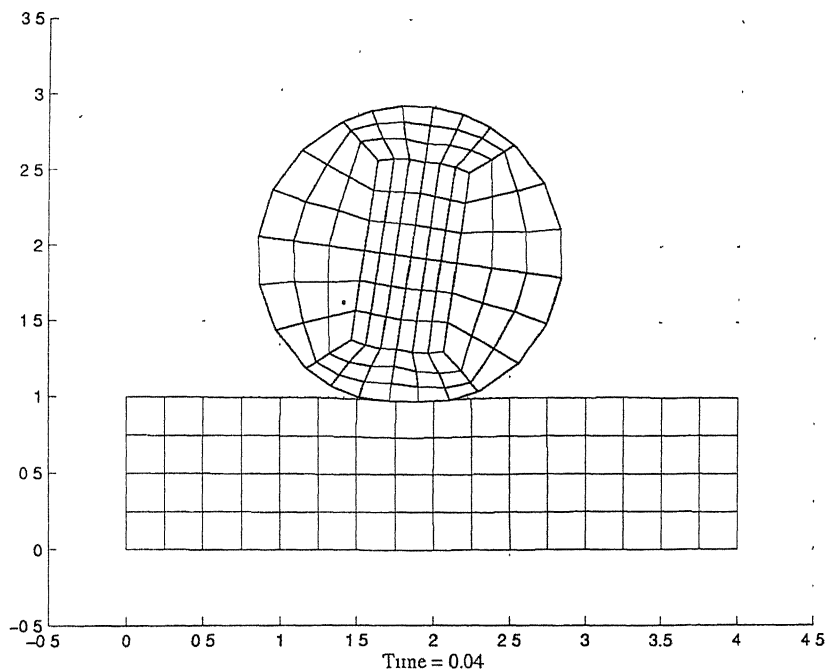


Figure 5.24: Impact of sphere on plate (Frictional): Configuration at $t = 0.04$

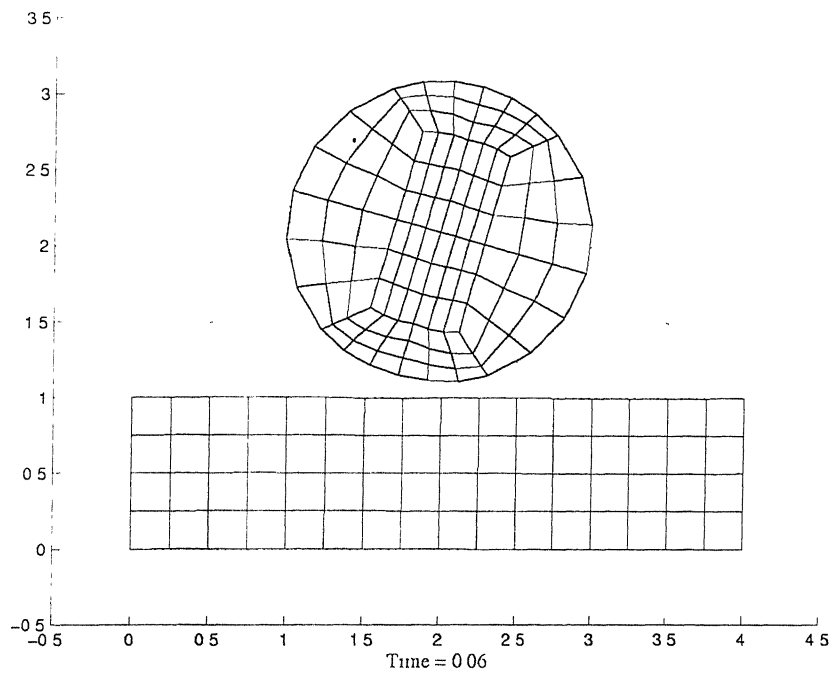


Figure 5.25: Impact of sphere on plate (Frictional): Configuration at $t = 0.06$

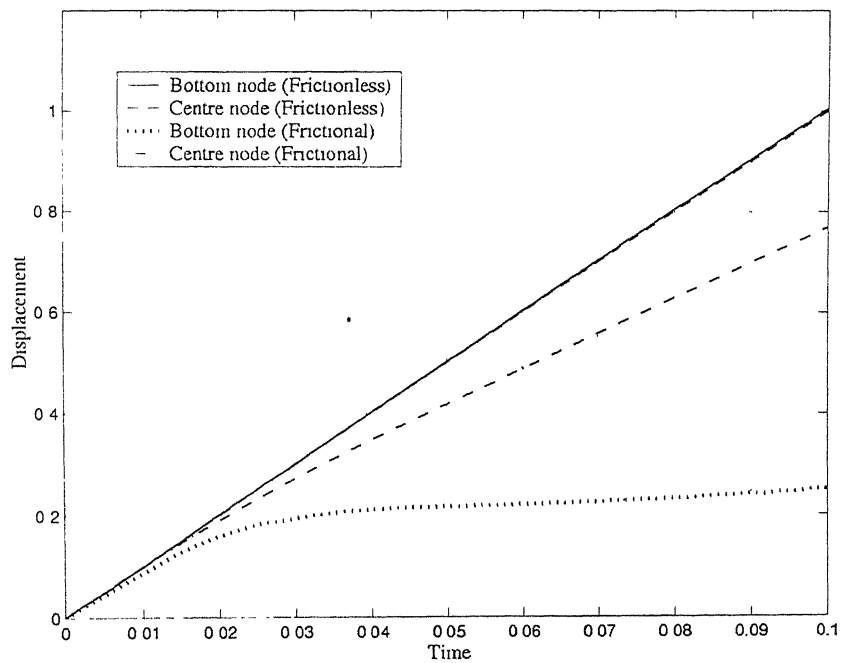


Figure 5.26: Displacement of the sphere along X-direction

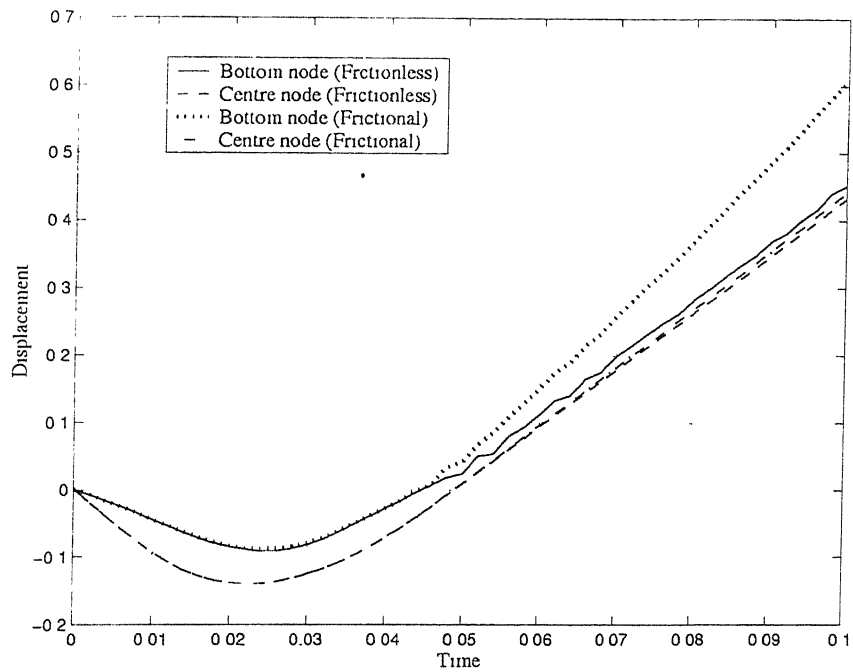


Figure 5.27: Displacement of the sphere along Z -direction

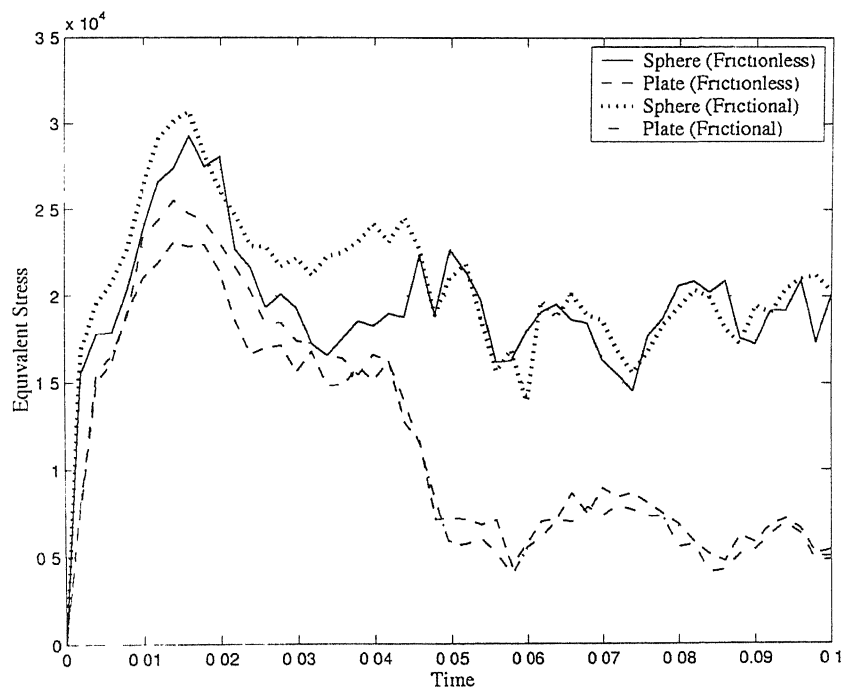


Figure 5.28: Maximum equivalent stress in sphere and plate

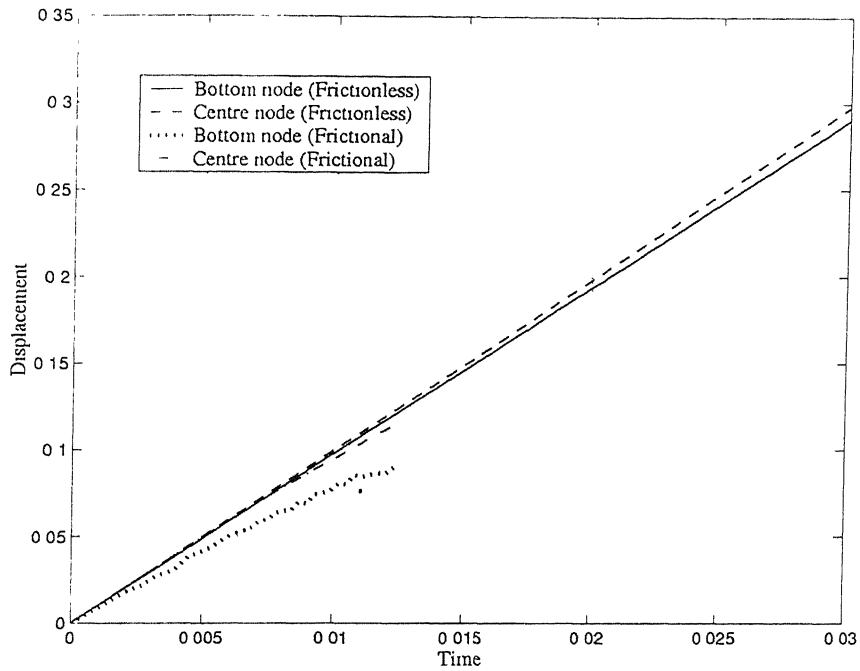


Figure 5.29: Displacement of the sphere along X -direction (polycarbonate material)

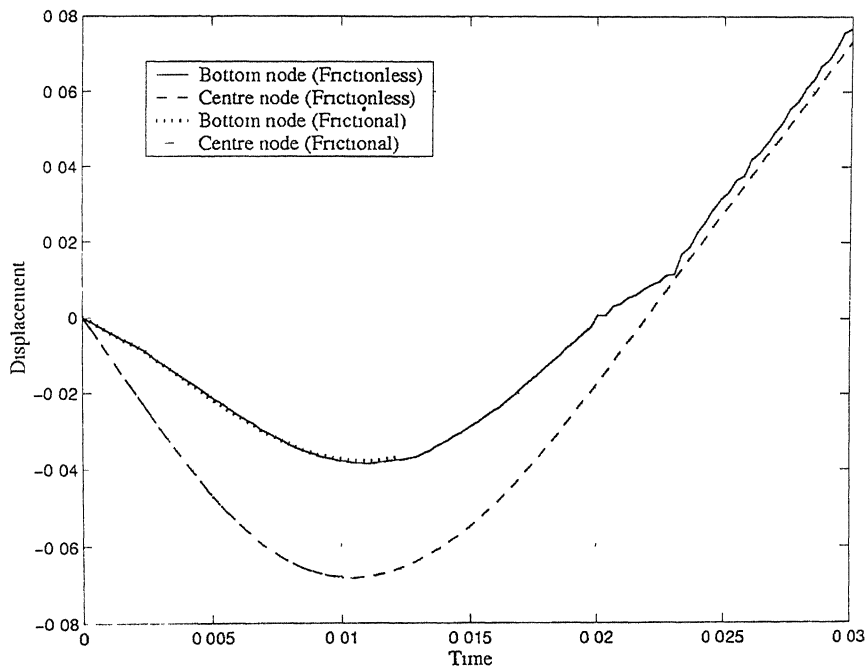


Figure 5.30: Displacement of the sphere along Z -direction (polycarbonate material)

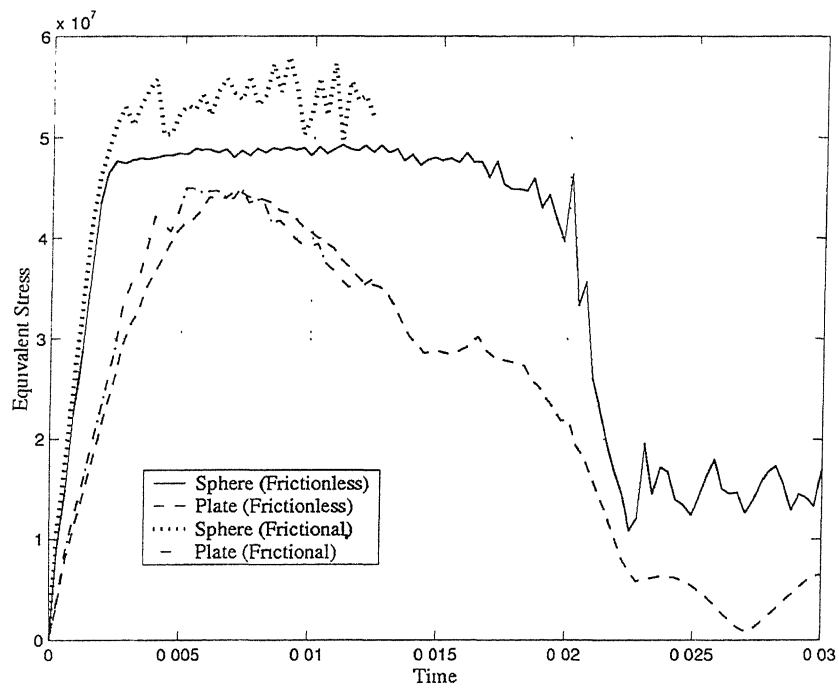


Figure 5.31: Maximum equivalent stress in sphere and plate (polycarbonate material)

Chapter 6

Conclusions and Scope for Future Work

6.1 Conclusions

A finite element code is developed for solving 3-D, dynamic, elasto-plastic contact problem including the effects of friction at the contact interface. A node-to-segment contact formulation is used for developing the contact stiffness matrix. The Lagrange multiplier method is used for enforcing the contact constraints. Frictional effects are included using the classical Coulomb's friction law. The updated Lagrangian formulation along with the modified Newton-Raphson iterative scheme is used for carrying out the elasto-plastic analysis. Divergence handling procedures, viz., under-relaxation and line search methods are incorporated to improve the convergence characteristics of Newton-Raphson iterations. Green-Lagrange strain tensor and objective Jaumann stress measure are used in the formulation of the governing equations. Elasto-plastic behaviour is modelled by an associated flow rule based on von Mises yield criterion and power law type isotropic hardening. Euler forward integration is used for the integration of the constitutive equation. Newmark's method, which is the best finite difference method in terms of stability and accuracy, is used for the time integration. An unloading scheme is incorporated to include the effect of local or global unloading.

The code is first validated by solving some standard problems, for which, the results are available in the published literature. Then one additional problem, the elasto-plastic impact of sphere on an elasto-plastic plate is solved to demonstrate the applicability of

the program. Therefore, this program can be used for analysing the practical problems.

6.2 Scope for Future Work

The desired future extensions of this work are the following:

1. Currently the program uses Green-Lagrange strain measure and Jaumann stress measure. Other strain and stress measures can be incorporated and comparative study of the results can be performed.
2. Other types of finite elements can be incorporated.
3. Material damping effects can be included.
4. Option for using penalty function method for developing the contact stiffness matrix can be incorporated.
5. Other material models like kinematic and anisotropic hardening and hardening laws other than power law can be implemented.
6. Non-classical friction laws can be used for modelling the effect of friction.
7. Finally, it is highly desirable to have versatile pre and post processors, so that the program can be more user-friendly.

References

- [1] R. Hill. *The Mathematical Theory of Plasticity*. Oxford University Press, Oxford, 1950.
- [2] L. E. Malvern. *Introduction to the Mechanics of a Continuous Medium*. Prentice Hall Inc., Englewood Cliffs, New Jersey, 1969.
- [3] O. C. Zienkiewicz, X. K. Li, and S. Nakazawa. Dynamic transient analysis by a mixed iterative method. *Int. J. Numer. Methods Eng.*, 23:1343, 1986.
- [4] K. J. Bathe. *Finite Element Procedures*. Prentice Hall of India, New Delhi, 1996.
- [5] J. H. Argyris. Elasto-plastic matrix displacement analysis of three dimensional continua. *J. Roy. Aero. Soc.*, 69:633, 1965.
- [6] J. C. Nagtegaal and J. E. De Jong. Some computational aspects of elastic-plastic large strain analysis. *Int. J. Numer. Methods Eng.*, 17:15, 1981.
- [7] M. A. Crisfield. *Non-linear Finite Element Analysis of Solids and Structures*, volume 1. John Wiley and Sons, Chichester, 1994.
- [8] J. Chakrabarty. *Theory of Plasticity*. McGraw Hill, New York, 1981.
- [9] E. H. Lee. Elastic-plastic deformation at finite strains. *J. Appl. Mech.*, 36:1, 1969.
- [10] I. Doghri. *Mechanics of Deformable Solids*. Springer, 2000.
- [11] K. J. Bathe, E. Ramm, and E. L. Wilson. Finite element formulations for large deformation dynamic analysis. *Int. J. Numer. Methods Eng.*, 9:353, 1975.
- [12] D. P. Mondkar and G. H. Powell. Finite element analysis of non-linear static and dynamic response. *Int. J. Numer. Methods Eng.*, 11:499, 1977.

- [13] A. S. Gendy and A. F. Saleeb. Mixed finite element modeling for the dynamics of beam assemblages undergoing large overall motions in space. *Int. J. Computational Engg. Science*, 2(2):309, 2001.
- [14] H. Hertz. On the contact of elastic solids. *Jr. of Math.*, 92:156, 1881. (in German).
- [15] K. L. Johnson. One hundred years of Hertz contact. In *Proceedings of Instn. of Mech. Engg.*, volume 196, page 363, 1982.
- [16] N. I. Muskhelishvili. *Some basic Problems of Mathematical Theory of Elasticity*. Noordhoff, Groningen, 1953.
- [17] G. M. L. Gladwell. *Contact problems in the Classical Theory of Elasticity*. Sijthoff & Noordhoff, Alphen aan den Rijn, 1980.
- [18] S. Ohte. Finite element analysis of elastic contact problems. *Bulletin of JSME*, 16(95):797, 1973.
- [19] R. Gaertner. Investigation of plane elastic contact allowing for friction. *Comput. Struct.*, 7:59, 1977.
- [20] A. Francavilla and O. C. Zienkiewicz. A note on numerical computation of elastic contact problems. *Int. J. Num. Methods Eng.*, 9:913, 1975.
- [21] T. D. Sachdeva and C. V. Ramakrishnan. A finite element analysis for the two-dimensional elastic contact problems with friction. *Int. J. Num. Methods Eng.*, 17:1257, 1981.
- [22] J. J. Kalker and Y. van Randen. A minimum principle for frictionless elastic contact with application to non-Hertzian half-space contact problem. *Jr. Engg. Math.*, 6:193, 1972.
- [23] N. D. Hung and G. de Saxce. Frictionless contact of elastic bodies by finite element method and mathematical programming technique. *Comput. Struct.*, 11:55, 1980.
- [24] F. F. Mahmoud, A. K. Al-Saffer, and A. M. El-Hadi. Solution of the non-conformal unbounded contact problems by the incremental convex programming method. *Comput. Struct.*, 39(1/2):1, 1991.

- [25] J. Bohm. A comparison of different contact algorithms with applications. *Comput. Struct.*, 26(1/2):207, 1987.
- [26] N. G. Bourago. A survey on contact algorithms. In *Workshop "Grid Generation: Theory and Applications"*, Moscow, 2002.
- [27] N. Kikuchi and J. T. Oden. *Contact Problems in Elasticity, A Study of Variational Inequality and Finite Element Methods*. SIAM, Philadelphia, 1988.
- [28] K. J. Bathe and A. Chaudhary. A solution method for planar and axisymmetric contact problems. *Int. J. Numer. Methods Eng.*, 21:65, 1985.
- [29] P. Wriggers and J. C. Simo. A note on tangent stiffness for fully non-linear contact problem. *Comp. in App. Num. Meth.*, 1:199, 1985.
- [30] H. Parisch. A consistent tangent stiffness matrix for three-dimensional non-linear contact analysis. *Int. J. Numer. Methods Eng.*, 28:1803, 1989.
- [31] W. Chen and J. Yeh. Finite element analysis of finite deformation contact problems with friction. *Comput. Struct.*, 29(3):403, 1988.
- [32] F. J. Gallego and J. J. Anza. A mixed finite element model for elastic contact problem. *Int. J. Numer. Methods Eng.*, 28:1249, 1989.
- [33] Z. H. Zhong. *Finite Element Procedures for Contact-Impact Problems*. Oxford University Press, Oxford, 1993.
- [34] G. Gilardi and I. Sharf. Literature survey of contact dynamics modelling. *Mechanism and Machine Theory*, 37(10):1213, 2002.
- [35] J. H. Sung and B. M. Kwak. Large displacement dynamic analysis with frictional contact by linear complementarity formulation. *Comput. Struct.*, 80:977, 2002.
- [36] E. Bittencourt and G. J. Creus. Finite element analysis of three-dimensional contact and impact in large deformation problems. *Comput. Struct.*, 69:219, 1998.
- [37] T. C. Werner. Elasto-plastic impact of a cantilever beam using non-linear finite elements and event simulation. Master's thesis, Youngstown State University, 1998.

- [38] T. Belytschko and M. O. Neal. Contact-impact pinball algorithm with penalty and Lagrangian methods. *Int. J. Numer. Methods Eng.*, 31:547, 1991.
- [39] J. G. Malone and N. L. Johnson. A parallel finite element contact/impact algorithm for non-linear explicit transient analysis: Part I — search algorithm and contact mechanics. *Int. J. Numer. Methods Eng.*, 37:559, 1994.
- [40] K. Brown, S. Attaway, S. Plimpton, and B. Hendrickson. Parallel strategies for crash and impact simulations. *Comput. Methods Appl. Mech. Engrg.*, 184:375, 2000.
- [41] R. L. Taylor and P. Papadopoulos. On a finite element method for dynamic contact/impact problems. *Int. J. Numer. Methods Eng.*, 36:2123, 1993.
- [42] T. A. Laursen and V. Chawla. Design of energy conserving algorithms for frictionless dynamic contact problems. *Int. J. Numer. Methods Eng.*, 40:863, 1997.
- [43] F. Armero and E. Petocz. A new dissipative time-stepping algorithm for frictional contact problems: Formulation and analysis. *Comput. Methods Appl. Mech. Engrg.*, 179:151, 1999.
- [44] M. L. Ayari and V. E. Saouma. Static and dynamic contact/impact problems using fictitious forces. *Int. J. Numer. Methods Eng.*, 32:623, 1991.
- [45] J. C. Simo and T. A. Laursen. An augmented Lagrangian treatment of contact problems involving friction. *Comput. Struct.*, 42(1):116, 1992.
- [46] C. Kane, E. A. Repetto, M. Ortiz, and J. E. Marsden. Finite element analysis of nonsmooth contact. *Comput. Methods Appl. Mech. Engrg.*, 180:1, 1999.
- [47] K. Farahani, M. Mofid, and A. Vafai. A solution method for general contact-impact problems. *Comput. Methods Appl. Mech. Engrg.*, 187:69, 2000.
- [48] O. C. Zienkiewicz. *The Finite Element Method*. Tata McGraw-Hill, New Delhi, 2001.
- [49] A. S. Gendy and A. F. Saleeb. Nonlinear dynamics for mixed shells with large rotation and elastoplasticity. *Int. J. Computational Engg. Science*, 1(1):1, 2000.
- [50] Kuldeep Bhat. Finite element analysis of dynamic elasto-plastic contact problem. Master's thesis, Department of Mechanical Engineering, IIT Kanpur, 2002.

A

1 2 3 4 5



A143471